

Responses to Reviewer Comments on acp-2015-237

Emissions of nitrogen oxides from US urban areas: estimation from Ozone Monitoring Instrument retrievals for 2005–2014

Z. Lu, D. G. Streets, B. de Foy, L. N. Lamsal, B. N. Duncan, and J. Xing

We thank all referees for their positive and constructive suggestions and comments, which have helped us improve the manuscript. All comments have been carefully dealt with, as detailed below, and we have highlighted all the changes in the revised manuscript (green for referee #1 and yellow for referee #2).

To Referee #1

This paper presents an interesting and valuable assessment NO_x emissions based on OMI observations. The strategy for using wind observations building on Valin et al.'s initial insight is nicely explained and results in emissions estimate that are significantly different from prior estimates. The paper should be published.

The one larger concern I have is with the absence of a discussion of possible remaining systematic errors. The authors have identified a substantial systematic error in prior emissions estimates (and trends) and explained the error arises by using OMI observations under all wind conditions. I wonder whether they think other significant systematic errors remain. Examples: Weekend vs. weekday emissions, a priori correlated with winds, chemical feedbacks . . .

Response Obtaining a sufficient number of samples is the major obstacle in this work to studying the weekend/weekday emission impact. Because all OMI measurements are divided on the basis of the wind speed, we have made our filter criteria as relaxed as possible and even combined all the valid data in three consecutive years to increase the amount of valid OMI data. If we further divided the OMI measurements by weekend/weekday, we would not have sufficient samples in the dataset, particularly for the weekend.

The potential systematic errors in wind field selected and the treatment of the wind field seem to be minor. First, the choice of wind field datasets was reported to be insensitive to the EMG results (Valin et al., 2013). This was further confirmed by de Foy et al. (2015) who tested wind fields of both the ERA-interim reanalysis (the one used in the current work) and the North American Regional Reanalysis (NARR) and obtained similar results in the EMG analysis. Second, although we choose fixed 12:00 LT as the time of the wind field, based on the work of Beirle et al. (2011), if the average wind over the last 6 hours is considered, the results only change slightly (~10%). Overall, Beirle et al. (2011) estimate the uncertainties due to the choice for the wind data as 30%, and we have taken that into account in the current analysis.

The chemical feedback of NO_x chemistry is somewhat related to the wind speed (i.e., slow or fast), because if there was no non-linearity of NO_x chemistry, there should be no significant differences between NO₂ trends derived from the all-wind and the weak wind situations. Please refer to our responses to the second and the third comments of Reviewer #2. In the revised manuscript, we have added a discussion of the possible relationship between the wind speed and the non-linear NO_x chemistry at the end of the last paragraph of Sect. 3.1.

Other minor issues: >On p. 14976, lines 10-15, the paper describes the procedure for filtering by wind speed and ensuring sufficient OMI observations. de Foy et al. (2014) does show that the EMG method generally gives the same answer for emission rate once the wind speed is greater than 3 m/s. Given this, why not take all winds >3 m/s rather than vary the cut off? Was this to be more consistent with Valin et al. (2013) where the number of OMI observations made it possible? Would always using 3 m/s change the results very much?

Response We will first briefly summarize the findings of de Foy et al. (2014) and Valin et al. (2013), and then give our consideration about the cut-off wind speed in this work. In de Foy et al. (2014), we evaluated the performance of the EMG method using simulated column densities over a point source with known emissions under three chemical lifetime cases (i.e., ∞ , 12-h, and 1-h). Generally, the EMG method provides reliable emission estimates at wind speeds >3 m/s in all lifetime cases. However, the EMG-obtained emissions seem to be more accurate when wind speeds are higher, especially for the 1-h chemical lifetime case (see Table 2 of de Foy et al., 2014).

In Valin et al. (2013), although they inferred NO_x emissions in the city of Riyadh from the OMI measurements with wind speeds >6.4 m/s only, their NO₂ burden and lifetime estimates at wind speeds >6.4 m/s were same as those at wind speeds >5 m/s (see bottom panel of Figure 4 of Valin et al., 2013). It implies that, instead of 6.4 m/s, using the cut-off wind speed of 5 m/s in their analysis would infer the same NO_x emission estimates of Riyadh. However, their mass balance calculations further showed that the NO₂ lifetime increased with decrease of the wind speed, implying the inaccuracy of NO_x emission estimates when using wind speeds slower than 5 m/s.

Taking into account the results of both of these studies, we choose to use 5 m/s (if possible) as the cut-off wind speed in this work because it should provide us with the most accurate emission estimates. For urban areas that don't have enough (i.e., at least 30 in three consecutive years) valid OMI samples due to this wind speed criterion, we relaxed the cut-off to 4 or 3 m/s. In fact, we did examine the results of using a fixed cut-off wind speed of 3 m/s and the differences are minor. In the revised manuscript, we have added two sentences here (i.e., the first paragraph of Sect. 3.2) to make the expressions clearer.

>Is the “fitting interval” (p. 14978, line 21) x_0 , sigma, or something else? If it is x_0 , then what is the difference between the effective and dispersion lifetimes? Is it that the effective lifetime is obtained at high wind speeds and the dispersion lifetime at low wind speeds?

Response The “fitting interval” is neither x_0 nor sigma. It is the dimension of the fitting domain downwind from the urban center, and it is used to calculate $\tau_{\text{dispersion}}$, which is further used to explain the differences between $\tau_{\text{residence}}$ obtained at low wind speeds and $\tau_{\text{effective}}$ obtained at high wind speeds (de Foy et al., 2014, 2015). We have made changes in the revised manuscript to make this clear.

>The discussion of NO_x lifetimes on pp. 14977-14978 is secondary to the main discussion of the correlation between the various emissions and burden trends, so it seems out of place in the middle of a section on emissions. Maybe it should be moved to the end of that section, or given its own (albeit short) section?

Response We agree with the reviewer that the discussion of the NO_x lifetimes seems out of place in the middle of Sect. 3.2. In the revised manuscript, we have moved this part to the end of Sect. 3.2.

>p. 14975 – lines 12-15. when discussing trends from weak wind data, is it meant to isolate the trends in the NO₂ column/burdens specifically? This sentence could be clarified as “we utilize OMI data under weak wind conditions to calculate the satellite-observed NO₂ columns, burdens, and trends in these quantities in this work.” This would just make clear that weak wind data is not being used to calculate trends in OMI-derived emissions.

Response The manuscript has been changed as suggested.

>p. 14977 – lines 9-10. Consider rewording as “and trends in NO₂ columns obtained at slow winds may better reflect the real bottom-up NO_x emissions trends.” This helps make clear that that column measurements at weak winds are being used as an indication of trends in surface emissions, rather than the strong-wind method of deriving emissions directly.

Response The manuscript has been changed as suggested.

>p. 14977 – lines 20-21. What exactly is meant by statistically significant in this context? Is it just that the columns are observable over background given the precision of the OMI measurements?

Response The term “statistically significant” here means that the uncertainty of the OMI burden estimated based on the method described in this work is less than 100% (including the impact of the precision of the OMI measurements).

To Referee #2

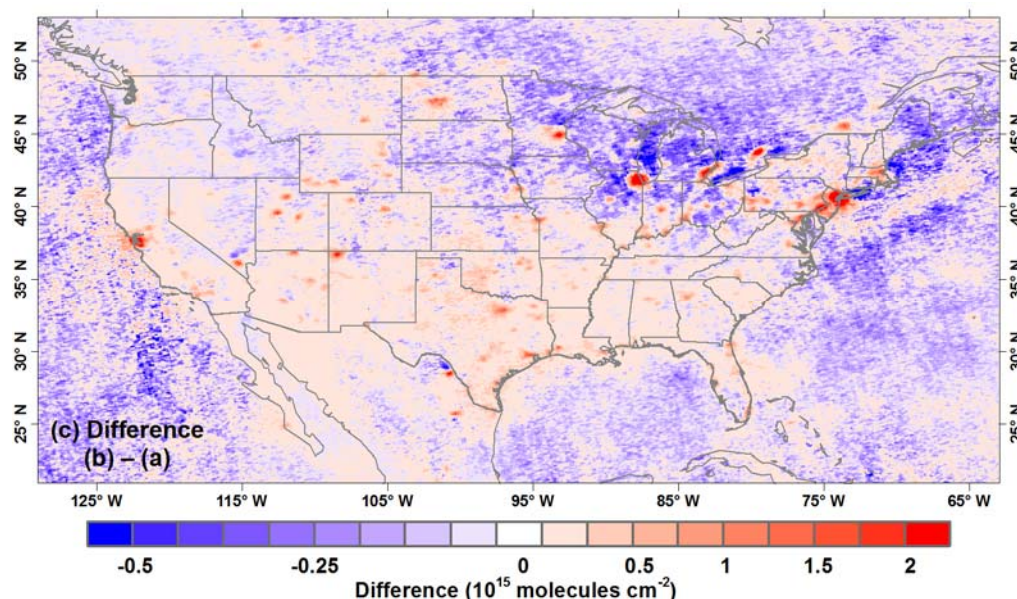
In their paper “Emissions of nitrogen oxides from US urban areas: estimation from Ozone Monitoring Instrument retrievals for 2005–2014“, Lu et al. report on an analysis of OMI satellite observations of tropospheric NO₂ column amounts over the US yielding detailed emission estimates for 35 major urban areas. This study builds on earlier work by Beirle et al. and Valin et al. but extends on it by using low wind speed situations to better estimate the absolute NO₂ burden and applying the effective life time derived from high wind speed scenarios after rotation by wind direction. The results show very good correlation with the absolute emissions from bottom-up estimates and also with their temporal evolution. The paper is well written, reports on an interesting and thorough study of satellite derived emission estimates and fits well into the scope of ACP. I therefore recommend it for publication after minor revisions.

Comments

- *One of the interesting aspects of this paper is the comparison of NO₂ columns taken at different wind speeds. As expected, NO₂ columns are larger in urban areas at low wind speed which is relevant for emission estimates and interpretation of satellite maps. However, I’m surprised to see that in Figure*

1c, there is not the expected ring of low (blue) values around the hot-spots. On the contrary, NO₂ levels appear to be higher nearly everywhere at low wind speed with the exception of the Great Lakes area. Do you have any explanation for this?

Response The differences between OMI NO₂ maps of an urban area at the all-wind-speed condition and at the slow-wind-speed condition depend on the local average wind speed. The higher the average wind speed, the larger the differences. In the US, the annual average wind speeds are relatively high in the northeast region (i.e., the Great Lakes area the reviewer mentioned), and therefore, the low NO₂ regions around the hotspots are more obvious in the northeast areas of the US. The figure below is a reproduction of Figure 1c with a different color bar scale from -0.5 to 2×10^{15} molecules/cm². The low-value regions can be seen around nearly all hotspots.



- As pointed out in the manuscript, not only the NO₂ columns over urban areas are larger at low wind speed, but also their relative changes over time. This is interesting but not explained in the paper. In my opinion, one explanation could be that at high NO₂ levels, the non-linearity in NO₂ lifetime increases the observed trends as under polluted conditions, the same reduction in NO_x emissions leads to larger reductions in NO₂ columns as it would under cleaner conditions. If this is the case, I would argue that the larger trends reported in this study are not necessarily an improvement over values derived from all wind conditions.*

Response We agree with the reviewer that larger NO₂ column reductions observed over urban areas at low wind-speed condition may be related to the non-linearity of the NO_x chemistry. At fast speed winds, the decreased NO₂ level over polluted urban areas may increase the NO_x lifetime so that the same reduction in NO_x emissions would lead to a smaller reduction in NO₂ columns compared to the slow wind-speed conditions. In the revised manuscript, we have added this possible explanation/discussion at the end of the last paragraph of Sect. 3.1.

However, we did not assert in the original manuscript that “the larger trends reported in this study

are ... an improvement over values derived from all wind conditions”. Our points are: (1) the presence of strong winds changes the observed NO₂ trends over a number of US urban areas (i.e., greater NO₂ reductions are observed under the weak-wind condition than under the all-wind condition) (e.g., the last paragraph of Sect. 3.1 in the original manuscript); and (2) trends in NO₂ columns obtained at slow winds may better reflect the real bottom-up NO_x emission trends (e.g., the second paragraph of Sect. 3.2 in the original manuscript). Therefore, in terms of constraining emission trends, based on our results and discussion in Sect. 3.1 and 3.2 of the original manuscript, we suggest using OMI NO₂ data at slow wind speeds when comparing to the bottom-up emission trends.

- *Also with respect to the difference in emission estimates at different wind speeds I would assume that in the absence of non-linearities in NO_x chemistry, there should not be a difference in NO_x emissions or trends derived from all wind situations if the averaging areas are large enough (as usually was the case in previous studies).*

Response In the absence of non-linearity of NO_x chemistry, if there is no significant interannual variation in wind fields and if the averaging areas are large enough, we agree with the reviewer that there should not be significant differences in NO_x emission trends and NO₂ trends derived from all-wind situations or NO₂ trends derived from weak-wind situations. However, NO_x chemistry is nonlinear and there are interannual variations in the meteorological field. Both factors make the NO₂ trends derived from the all-wind condition differ from the NO_x emission trends. Our trends comparison in the second paragraph of Sect. 3.2 and the third paragraph of Sect. 3.3 of the original manuscript clearly shows that NO₂ decreasing trends in US urban areas obtained at slow winds are greater than the previously reported values obtained in all-wind conditions, and, more importantly, are closer to both the “top-down” EMG-derived NO_x emission trends and the “bottom-up” NEI NO_x emission trends, as well as surface NO₂ trends.

- *The discussion of uncertainties is in my opinion somewhat misleading as the effect of cancellation of some systematic errors in trend analysis is not taken into account. As a result, all changes in OMI derived quantities over time shown in Figure 5 are smaller than the error bars which would make them non-significant. I think this should be improved.*

Response In this work, we use exactly the same uncertainty analysis method as previous EMG-related studies such as Beirle et al. (2011) and Ialongo et al. (2014), and the terms “uncertainty” or “error” refer to one standard deviation (SD) or the coefficient of variation (SD divided by the mean) of the estimated results throughout the manuscript. From this point of view, we prefer to keep the current meaning of error bars in Figure 5. For clarification, in the revised manuscript, we have emphasized in the caption of Figure 5 that “error bars express the ± 1 SD of the annually estimated results”.

- *I do not see the point of Figure 8 and recommend to remove it.*

Response We still prefer to keep this figure in the current work. Figure 8 shows the sum of OMI NO₂ columns for all urban areas, and it represents the direct OMI NO₂ measurements. From this figure, we can clearly see the decrease and the pace of OMI NO₂ observations over selected US urban areas, and it supports two aspects of our discussion in Sect. 3.3. Though similar, “OMI NO₂ column” is different

from another quantity used in this work “OMI NO₂ burden”, because the latter is not a direct measurement but a fitted result from the EMG method.

Technical Comments

- *p14963, 119: inventories of NO_x -> inventories of NO_x emissions*

Response The manuscript has been revised correspondingly.

- *p14963, 120: bottom up inventories are uncertain but I would guess that both fuel type and technology are rather well constrained*

Response We respectfully disagree with the reviewer at this point. Even in the US, fuel type and technology are not well constrained in some sectors: the fleet of US vehicles and residential biomass burning, for example.

- *p14963, 125: not sure if current satellites really have “high temporal and spatial resolution” for NO₂*

Response Take the OMI onboard the NASA-Aura satellite as an example. It has been continuously providing us NO₂ measurements at daily global coverage with the smallest pixel size of 13 km by 24 km in the past ten years. We understand that the reviewer might be unsure about whether this could be called “high temporal and spatial resolution”. Therefore, we have removed this expression in the revised manuscript.

- *p14965, 124: (also elsewhere) as there are several OMI NO₂ retrievals, I would replace “the OMI NO₂ retrievals” by “OMI NO₂ retrievals” or “TEMIS OMI NO₂ retrievals”*

Response The manuscript has been revised as suggested.

- *p14966, 110: the multi-annual -> a multi-annual*

Response The manuscript has been revised correspondingly.

- *p14967, 119: make -> makes*

Response The manuscript has been revised correspondingly.

- *p14967, 123: “to smooth” – I don’t think that a high sampling rate smooths the data – better sampling will lead to smoother looking averages but in fact, the level of details is higher, not lower as after smoothing.*

Response In the revised manuscript, this sentence has been revised to “all the valid pixels were oversampled on a 2 km × 2 km grid to obtain detailed spatial distributions of NO₂ over hotspots”. Averaging a large number of OMI pixel data (the smallest pixel size 13 km × 24 km) to fine grids (e.g., 2 km × 2 km in this work) does help us see the detailed spatial distribution of NO₂ plumes over hot spots (see Russell et al., 2010; Fioletov et al., 2011, 2013; de Foy et al., 2009; Lu et al., 2013).

- *p14968, 116: Please add spatial resolution of ERA-interim data in km for comparison with your 2 km sampling grid*

Response We use the gridded ERA-interim data at the resolution of 0.5 degree in this work and this information has been added in the revised manuscript.

- *p14968, l25: I think this point deserves a little bit more discussion – if the NO₂ plume of a point source depends on the evolution of wind speed over the last hours, why is it OK to just take the wind field at one (interpolated) time, arbitrarily selected to be 12:00 LT?*

Response First, the choice of 12:00 LT has been proven to successfully reproduce the observed spatial transport pattern of the OMI NO₂ at the daily level (Valin et al., 2013). Second, based on the work of Beirle et al. (2011), if, instead, the average wind over the last 6 hours is considered, the results only change slightly (~10%). Therefore, for simplicity, we choose 12:00 LT as the time of the wind fields. Please also note that we assigned 30% uncertainty to the wind data. In the revised manuscript, we have added some discussion in the last paragraph of Sect. 2.3 to reflect this point.

- *p14969, l10: and the longitudes -> and longitudes*

Response The manuscript has been revised correspondingly.

- *p14969, l14: one-dimension -> one-dimensional*

Response The manuscript has been revised correspondingly.

- *p14970, l16: parameter -> parameters*

Response The manuscript has been revised correspondingly.

- *p14970, l20: “we made additional treatments in processing” sounds odd to me*

Response In the revised manuscript, this sentence has been revised to “We made additional treatments to the OMI NO₂ data when using the EMG method”.

- *p14971, l1: the north-westerly -> north-westerly*

Response The manuscript has been revised correspondingly.

- *p14972, l12: countries -> counties*

Response The manuscript has been revised correspondingly.

- *p14973, l2: inclusive -> included*

Response The manuscript has been revised correspondingly.

- *p14974, l20: in sum -> in summary*

Response The manuscript has been revised correspondingly.

- *p14985, l10: While I agree that “a comprehensive and integrated analysis of satellite observations, ground-based measurements, and bottom-up emissions can overcome shortcomings of the individual datasets”, I don’t think this has been done in the manuscript at hand.*

Response This sentence has been revised to “a comprehensive and integrated analysis of satellite observations, ground measurements, and bottom-up emissions can provide a better understanding of the true NO_x situation in a given area” in the revised manuscript.

References

- Beirle, S., Boersma, K. F., Platt, U., Lawrence, M. G., and Wagner, T.: Megacity emissions and lifetimes of nitrogen oxides probed from space, *Science*, 333, 1737–1739, 2011.
- de Foy, B., Krotkov, N. A., Bei, N., Herndon, S. C., Huey, L. G., Martinez, A. P., Ruiz-Suarez, L. G., Wood, E. C., Zavala, M., and Molina, L. T.: Hit from both sides: tracking industrial and volcanic plumes in Mexico City with surface measurements and OMI SO₂ retrievals during the MILAGRO field campaign, *Atmos. Chem. Phys.*, 9, 9599–9617, 2009.
- de Foy, B., Wilkins, J. L., Lu, Z., Streets, D. G., and Duncan, B. N.: Model evaluation of methods for estimating surface emissions and chemical lifetimes from satellite data, *Atmos. Environ.*, 98, 66–77, 2014.
- de Foy, B., Lu, Z., Streets, D. G., Lamsal, L. N., and Duncan, B. N.: Estimates of power plant NO_x emissions and lifetimes from OMI NO₂ satellite retrievals, *Atmos. Environ.*, 116, 1–11, 2015.
- Fioletov, V. E., McLinden, C. A., Krotkov, N., Moran, M. D., and Yang, K.: Estimation of SO₂ emissions using OMI retrievals, *Geophys. Res. Lett.*, 38, L21811, doi:10.1029/2011gl049402, 2011.
- Fioletov, V. E., McLinden, C. A., Krotkov, N., Yang, K., Loyola, D. G., Valks, P., Theys, N., Van Roozendaal, M., Nowlan, C. R., Chance, K., Liu, X., Lee, C., and Martin, R. V.: Application of OMI, SCIAMACHY, and GOME-2 satellite SO₂ retrievals for detection of large emission sources, *J. Geophys. Res.*, 118, 11399–11418, 2013.
- Ialongo, I., Hakkarainen, J., Hyttinen, N., Jalkanen, J. P., Johansson, L., Boersma, K. F., Krotkov, N., and Tamminen, J.: Characterization of OMI tropospheric NO₂ over the Baltic Sea region, *Atmos. Chem. Phys.*, 14, 7795–7805, 2014.
- Lamsal, L. N., Martin, R. V., Padmanabhan, A., van Donkelaar, A., Zhang, Q., Sioris, C. E., Chance, K., Kurosu, T. P., and Newchurch, M. J.: Application of satellite observations for timely updates to global anthropogenic NO_x emission inventories, *Geophys. Res. Lett.*, 38, L05810, doi:10.1029/2010gl046476, 2011.
- Lu, Z., Streets, D. G., de Foy, B., and Krotkov, N. A.: Ozone Monitoring Instrument observations of interannual increases in SO₂ emissions from Indian coal-fired power plants during 2005–2012, *Environ. Sci. Technol.*, 47, 13993–14000, 2013.
- Russell, A. R., Valin, L. C., Bucsela, E. J., Wenig, M. O., and Cohen, R. C.: Space-based constraints on spatial and temporal patterns of NO_x emissions in California, 2005–2008, *Environ. Sci. Technol.*, 44, 3608–3615, 2010.

Valin, L. C., Russell, A. R., and Cohen, R. C.: Variations of OH radical in an urban plume inferred from NO₂ column measurements, *Geophys. Res. Lett.*, 40, 1856-1860, 2013.

Emissions of nitrogen oxides from U.S. urban areas: estimation from Ozone Monitoring Instrument retrievals for 2005–2014

Zifeng Lu^{1,*}, David G. Streets¹, Benjamin de Foy², Lok N. Lamsal^{3,4}, Bryan N. Duncan⁴, and Jia Xing⁵

¹ Energy Systems Division, Argonne National Laboratory, Argonne, IL 60439, USA

² Department of Earth and Atmospheric Sciences, Saint Louis University, St. Louis, MO 63108, USA

³ Goddard Earth Sciences Technology and Research, Universities Space Research Association, Columbia, MD 21046, USA

⁴ NASA Goddard Space Flight Center, Greenbelt, MD 20771, USA

⁵ US Environmental Protection Agency, Research Triangle Park, NC 27711, USA

Manuscript submitted to

Atmospheric Chemistry and Physics

September 1, 2015

The submitted manuscript has been created by UChicago Argonne, LLC, Operator of Argonne National Laboratory ("Argonne"). Argonne, a U.S. Department of Energy Office of Science laboratory, is operated under Contract No. DE-AC02-06CH11357. The U.S. Government retains for itself, and others acting on its behalf, a paid-up nonexclusive, irrevocable worldwide license in said article to reproduce, prepare derivative works, distribute copies to the public, and perform publicly and display publicly, by or on behalf of the Government.

* Corresponding author: Tel: 630-252-9853; Fax: 630-252-8007; Email: zlu@anl.gov

Emissions of nitrogen oxides from U.S. urban areas: estimation from Ozone Monitoring Instrument retrievals for 2005–2014

Zifeng Lu¹, David G. Streets¹, Benjamin de Foy², Lok N. Lamsal^{3,4}, Bryan N. Duncan⁴, and Jia Xing⁵

[1] Energy Systems Division, Argonne National Laboratory, Argonne, IL 60439, USA

[2] Department of Earth and Atmospheric Sciences, Saint Louis University, St. Louis, MO 63108, USA

[3] Goddard Earth Sciences Technology and Research, Universities Space Research Association, Columbia, MD 21046, USA

[4] NASA Goddard Space Flight Center, Greenbelt, MD 20771, USA

[5] US Environmental Protection Agency, Research Triangle Park, NC 27711, USA

Correspondence to: Z. Lu (zlu@anl.gov)

Abstract

Satellite remote sensing of tropospheric nitrogen dioxide (NO₂) can provide valuable information for estimating surface nitrogen oxides (NO_x) emissions. Using an exponentially-modified Gaussian (EMG) method and taking into account the effect of wind on observed NO₂ distributions, we estimate three-year moving-average emissions of summertime NO_x from 35 U.S. urban areas directly from NO₂ retrievals of the Ozone Monitoring Instrument (OMI) during 2005–2014. Following conclusions of previous studies that the EMG method provides robust and accurate emission estimates under strong-wind conditions, we derive top-down NO_x emissions from each urban area by applying the EMG method to OMI data with wind speeds greater than 3–5 m s⁻¹. Meanwhile, we find that OMI NO₂ observations under weak-wind conditions (i.e., <3 m s⁻¹) are qualitatively better correlated to the surface NO_x source strength in comparison to all-wind OMI maps; and therefore we use them to calculate

the satellite-observed NO₂ burdens of urban areas and compare with NO_x emission estimates. The EMG results show that OMI-derived NO_x emissions are highly correlated ($R>0.93$) with weak-wind OMI NO₂ burdens as well as with bottom-up NO_x emission estimates over 35 urban areas, implying a linear response of the OMI observations to surface emissions under weak-wind conditions. The simultaneous EMG-obtained effective NO₂ lifetimes ($\sim 3.5 \pm 1.3$ h), however, are biased low in comparison to the summertime NO₂ chemical lifetimes. In general, isolated urban areas with NO_x emission intensities greater than ~ 2 Mg h⁻¹ produce statistically significant weak-wind signals in three-year average OMI data. From 2005 to 2014, we estimate that total OMI-derived NO_x emissions over all selected U.S. urban areas decreased by 49%, consistent with reductions of 43%, 47%, 49%, and 44% in the total bottom-up NO_x emissions, the sum of weak-wind OMI NO₂ columns, the total weak-wind OMI NO₂ burdens, and the averaged NO₂ concentrations, respectively, reflecting the success of NO_x control programs for both mobile sources and power plants. The decrease rates of these NO_x-related quantities are found to be faster (i.e., -6.8 to -9.3% yr⁻¹) before 2010 and slower (i.e., -3.4 to -4.9% yr⁻¹) after 2010. For individual urban areas, we calculate the R values of pair-wise trends among the OMI-derived and bottom-up NO_x emissions, the weak-wind OMI NO₂ burdens, and ground-based NO₂ measurements, and high correlations are found for all urban areas (median $R=0.8$), particularly large ones (R up to 0.97). The results of the current work indicate that using the EMG method and considering the wind effect, the OMI data allow for the estimation of NO_x emissions from urban areas and the direct constraint of emission trends with reasonable accuracy.

1 Introduction

Nitrogen oxides (NO_x), the sum of nitrogen dioxide (NO₂) and nitric oxide (NO), is one of the six criteria pollutants identified by the U.S. Environmental Protection Agency (EPA) under the requirement of the Clean Air Act. NO_x plays a crucial role in tropospheric chemistry processes such as the formation of ground-level ozone and secondary inorganic and organic aerosols; and thus it is also linked with other criteria pollutants including ozone, particulate matter, carbon monoxide, and sulfur oxides. Therefore, NO_x is not only harmful to human health, but also implicated in a number of environmental problems, such as acid rain, smog, eutrophication, climate change, etc. NO_x emissions come from both anthropogenic (e.g., man-made combustion of fossil fuels, biofuel, and biomass) and natural sources (e.g., lightning,

1 microbial processes in soils, and wildfires). Bottom-up inventories of NO_x emissions can be
2 quite uncertain, because the emission factors of anthropogenic sources strongly depend on the
3 fuel type, technology, and combustion condition, while natural sources are inherently difficult
4 to quantify.

5 Due to the strong absorption of NO₂ molecules in the visible wavelength range of the
6 spectrum, satellite instruments based on the principle of optical absorption spectroscopy serve
7 as powerful tools to detect NO₂ signals from space (Martin, 2008 and references therein). The
8 short lifetime of NO_x in the atmosphere leads to a close correlation between observed NO₂
9 columns and surface NO_x emission sources, implying the potential of space-borne instruments
10 to aid in the estimation of NO_x emissions (Streets et al., 2013, 2014; and references therein).
11 In the past two decades, satellite remote sensing of tropospheric NO₂ columns has been
12 widely and successfully used to map the spatial distributions of NO₂ at local, regional, and
13 global scales (e.g., Kim et al., 2009; Russell et al., 2010; Boersma et al., 2007, 2011; Martin
14 et al., 2003), identify intensive point and area NO_x emission sources (e.g., Duncan et al.,
15 2013; Kim et al., 2006; Lu and Streets, 2012; Streets et al., 2014; Wang et al., 2010; Zhang et
16 al., 2009), and monitor diurnal/weekly/monthly/interannual variations of NO₂ (e.g., Hilboll et
17 al., 2013; Hudman et al., 2010; Richter et al., 2005; Russell et al., 2012; Schneider et al.,
18 2015; Tong et al., 2015; van der A et al., 2008) for both anthropogenic and natural sources.

19 In general, local, regional, and global NO_x emissions can be verified, estimated, and
20 optimized by using forward and inverse modeling of satellite NO₂ columns (e.g., Boersma et
21 al., 2005; Jaeglé et al., 2005; Kim et al., 2009; Martin et al., 2003; Wang et al., 2012).
22 However, NO_x emissions and NO₂ lifetimes can also be determined directly by analyzing the
23 downwind patterns of the satellite-observed NO₂ columns near the sources. Leue et al. (2001)
24 used an exponential function to fit the downwind decay of GOME (Global Ozone Monitoring
25 Experiment)-observed NO₂ columns at the eastern shore of the U.S. and estimated the NO₂
26 lifetime by using the fitted *e*-folding distance and the averaged wind velocity. Kunhikrishnan
27 et al. (2004) conducted a similar analysis over the Arabian Sea outflow region to estimate the
28 regional NO_x lifetime for the Indian subcontinent. This method was revised by Beirle et al.
29 (2004), who fitted the GOME-observed NO₂ columns across the shipping lane between Sri
30 Lanka and Indonesia with an exponentially-modified Gaussian (EMG) function and derived
31 the mean NO_x lifetime and the corresponding ship emissions for 1996–2001. Hereinafter, we
32 call this approach the EMG method. By fitting the downwind line densities of the OMI

(Ozone Monitoring Instrument)-observed NO₂ separately for eight wind directions, Beirle et al. (2011) further improved the EMG method and determined the average NO_x emissions and lifetimes simultaneously for nine worldwide megacities during 2005–2009. Using a similar method, Ialongo et al. (2014) estimated the average summertime NO_x emissions and lifetimes of three cities in the Baltic Sea region during 2005–2011. The EMG method and its variant versions have also been applied to the satellite observations of SO₂ to constrain SO₂ lifetimes and emissions from volcanoes (Beirle et al., 2014; Krotkov et al., 2010; Theys et al., 2013; Carn et al., 2013) and large anthropogenic point sources (Fioletov et al., 2015).

Recently, several studies discussed the applicability and reliability of the EMG method. Valin et al. (2013) suggested that the NO_x emissions and chemical lifetimes would be better quantified when winds are fast because the downwind NO₂ decay under this condition is dominated by chemical removal, not variability of the winds. Introducing the plume rotation technique, they inferred NO_x emissions of Riyadh from the OMI measurements with fast winds ($>6.4 \text{ m s}^{-1}$) only and derived NO_x chemical lifetimes in slower wind conditions with the mass balance method. Additionally, de Foy et al. (2014) evaluated the performance of the EMG method using simulated column densities over a point source with known emissions under three chemical lifetime cases. They found that the EMG method generally provided reliable emission estimates at fast wind-speed conditions ($>3 \text{ m s}^{-1}$); however, the lifetime estimates were biased low and quite sensitive to the selection of the wind speed cut-off and the accuracy of the plume rotation. This implies that, in practice, the EMG-derived lifetimes should not be treated as chemical lifetimes, but rather as “effective lifetimes” that include the influences of chemical conversion, plume meandering, grid resolution, sampling issues, etc. (see also Fioletov et al., 2015; Ialongo et al., 2014). Nevertheless, the EMG method can provide quite accurate emission estimates if the issues of wind speed and direction are appropriately treated.

In this study, we use OMI NO₂ retrievals and an EMG method to estimate NO_x emissions from 35 major U.S. urban areas during the OMI era of 2005–2014. Although there have been a number of studies reporting satellite observations of NO₂ over some U.S. cities, they mainly focused on the interannual trends and/or monthly/weekly variations of the satellite signals themselves (van der A et al., 2008; Hilboll et al., 2013; Schneider et al., 2015; Russell et al., 2012; Kim et al., 2009) or the comparison of satellite observations with pre-existing emissions and/or surface measurement datasets (Tong et al., 2015; Lamsal et al., 2015). In this

1 study, we use the EMG-method to estimate NO_x emissions of nearly all major U.S. cities
2 directly from satellite NO₂ observations and without using a chemical transport model. The
3 prime motivation of this work is not to demonstrate the well-known dramatic decrease of
4 urban NO₂ across the country (although we do have new findings by taking into account the
5 wind effect), but to show the capability of the EMG method to provide direct and reliable
6 estimates of urban NO_x emissions. The current work also differs from previous EMG-related
7 studies (Beirle et al., 2004, 2011; de Foy et al., 2014, 2015; Ialongo et al., 2014; Valin et al.,
8 2013), all of which used a multi-annual-averaged satellite NO₂ map in the EMG fit and thus
9 only obtained a long-term averaged emission estimate. This work, to our knowledge, is the
10 first study to show that the EMG method can also provide estimates of emission trends with
11 reasonable accuracy. The rest of the paper is organized as follows: Sect. 2 documents the
12 methodology and data sets; Sect. 3 highlights the effect of wind on the OMI NO₂ observations
13 (Sect. 3.1), presents the relationship between the EMG-derived NO_x emissions and the OMI
14 NO₂ observations (Sect. 3.2), and compares the trends of various NO_x-related quantities (Sect.
15 3.3); Sect. 4 summarizes the major findings of this work.

16

17 **2 Data and methodology**

18 **2.1 OMI NO₂ retrievals and processing**

19 The OMI is an ultraviolet/visible nadir spectrometer onboard the National Aeronautics and
20 Space Administration (NASA)'s Aura satellite, which was launched in a sun-synchronous
21 ascending orbit at 705 km altitude in July 2004 (Levelt et al., 2006). It measures solar
22 irradiance and earthshine radiance in the wavelength range of 270 to 500 nm and has been
23 continuously providing aerosol and gaseous (including NO₂) column observations at
24 approximately 13:45 local equator-crossing time with nearly daily global coverage in the past
25 decade. In this work, we use the version 2.0 product of the Dutch OMI NO₂ (DOMINO)
26 tropospheric vertical column densities (TVCDs) developed at the Royal Netherlands
27 Meteorological Institute (KNMI) for the years from 2005 to 2014 (Boersma et al., 2007,
28 2011). This version of the product uses an improved OMI NO₂ retrieval algorithm on the
29 basis of better air mass factors, an *a posteriori* correction for across-track stripes, and high-
30 resolution input profiles of the terrain height and the surface albedo climatology, and has been

1 reported to be in better agreement with independent measurements and model simulations in
2 comparison to the previous version (Boersma et al., 2011).

3 To increase the amount of valid OMI data, the filter criteria of the level-2 swath data were
4 relaxed somewhat. We removed the daily pixel retrievals with solar zenith angle >80 degrees,
5 cloud radiance fraction >0.5, or surface albedo >0.3. The largest five pixels at the swath edges
6 (i.e., rows 1 to 5 and rows 56 to 60) were excluded to limit the across-track pixel width to <70
7 km. Since June 2007, some row anomalies (RAs) have developed on the OMI detectors and
8 affected the data quality of a number of cross-track scenes
9 (<http://www.knmi.nl/omi/research/product/rowanomaly-background.php>). The RAs change
10 over time and we therefore dynamically removed the affected pixels based on the RA flags in
11 the DOMINO product. We only used the summer half-year data (i.e., April to September)
12 because the short NO_x lifetime in this period makes the relationship between NO_x emissions
13 and satellite NO₂ observations more direct than in other months (e.g., Russell et al., 2012;
14 Wang et al., 2012; Lu and Streets, 2012). For the OMI NO₂ maps of the entire domain of the
15 continental U.S. (e.g., Fig. 1a), all the valid pixels were oversampled on a 2 km × 2 km grid to
16 obtain detailed spatial distributions of NO₂ over hotspots (Lu et al., 2013; Russell et al., 2010;
17 Fioletov et al., 2011, 2013; de Foy et al., 2009).

18 [Fig. 1](#)

19 **2.2 Selection of urban areas**

20 Table 1 lists and Fig. 1a shows the locations of the urban areas selected in this work. We
21 examined the top 50 urban areas in the U.S. based on population size and the observed
22 satellite NO₂ signals (Fig. 1a). We combined adjacent urban areas that are so close as to share
23 the same NO₂ hotspot (e.g., Washington, DC, and Baltimore; and Los Angeles and Riverside)
24 and omitted some urban areas where the NO₂ signals are not isolated due to the influence of
25 large NO_x emitting sources nearby (e.g., Pittsburgh, Milwaukee, San Francisco). In total, 35
26 urban areas were selected for analysis, and they together accounted for ~23% of total NO_x
27 emissions and ~50% of total urban population in the U.S. during the period 2005–2014.

28 [Table 1](#)

2.3 Wind fields

Wind information (including speed and direction) is crucial in exploring its influence on the OMI NO₂ observations and estimating the NO_x emissions with the exponentially-modified Gaussian (EMG) method described in Sect. 2.4. In this work, we use the gridded wind field datasets of the ERA-interim reanalysis at the resolution of $0.5^\circ \times 0.5^\circ$ developed by the European Center for Medium-range Weather Forecast (ECMWF) (Dee et al., 2011). The ERA-interim reanalysis provides global wind fields for 60 vertical levels at four time steps per day (i.e., 0:00, 6:00, 12:00, 18:00 UTC) from 1979 to present on the N128 reduced Gaussian grid. Valin et al. (2013) expected that the EMG results would be insensitive to the choice of wind field datasets. This was confirmed by de Foy et al. (2015) who tested wind fields of both the ERA-interim reanalysis and the North American Regional Reanalysis (NARR) and obtained similar results in the EMG analysis. The NO_x emitted near the surface of the urban areas can undergo rapid vertical mixing, and we thus use the averaged wind fields of the bottom eight levels (i.e., from the surface to ~500 m), similar to the treatment of Beirle et al. (2011). We assume that the daily OMI NO₂ spatial pattern of a hotspot should not reflect the wind strength and direction at the OMI overpass time of ~13:45 LT, but the average wind fields a few hours before the satellite takes the measurement. For simplicity, we choose 12:00 LT as the time of the wind fields. The reasons are: first, the choice of 12:00 LT of the ERA-interim reanalysis dataset has been proven to reproduce the observed spatial transport pattern of the OMI NO₂ successfully at the daily level (Valin et al., 2013); second, if the average wind over the last 6 hours is considered, the results have been reported to change only ~10% (Beirle et al., 2011). Consequently, daily wind speed and wind direction maps over the entire domain of the U.S. were interpolated temporally at 12:00 LT and spatially on a 2 km × 2 km grid in association with the oversampled OMI NO₂ maps.

2.4 Exponentially-modified Gaussian method

Beirle et al. (2011) presented a method using an EMG function to fit the downwind patterns of OMI NO₂ line densities separately for eight wind directions and simultaneously determined the NO_x emissions and lifetimes for nine megacities around the world. In this work, we follow a similar methodology but with a number of enhancements. For each urban area, we did not separate the OMI NO₂ measurements into different wind directions, but rotated and overlapped the daily OMI NO₂ maps in the range of 300 km around the urban center (see

1 Table 1 for the latitudes and longitudes) to align all the wind directions at the urban center in
 2 the x -direction (Valin et al., 2013; de Foy et al., 2014, 2015). This process increases the
 3 number of OMI samples, potentially increases the signal-to-noise ratio, and benefits the trend
 4 analysis using the EMG method. The wind-aligned OMI NO₂ maps were further reduced to
 5 one-dimensional line densities by integrating the NO₂ data in the across-wind direction over a
 6 maximum interval of ± 120 km (e.g., Chicago in Fig. 2). Depending on the size of the urban
 7 areas, smaller across-wind integration intervals down to ± 60 km were chosen for smaller NO₂
 8 hotspots to minimize interference from background NO₂ and neighboring NO_x sources. The
 9 EMG model proposed by Beirle et al. (2011) was then used to fit the NO₂ line densities. As a
 10 function of the distance from the urban center x , the EMG model is expressed as Eq. (1) to
 11 (3):

$$12 \quad \text{OMI}_{\text{NO}_2, \text{line}}(x | \mu, \sigma, x_0, \alpha, B) = \alpha \cdot f(x | \mu, \sigma, x_0) + B = \alpha \cdot [e(x | x_0, \mu) \otimes G(x | \sigma)] + B \quad (1)$$

$$13 \quad e(x | x_0, \mu) = \exp\left(-\frac{x - \mu}{x_0}\right) \text{ for } x \geq \mu, \text{ otherwise } e(x | x_0, \mu) = 0 \quad (2)$$

$$14 \quad G(x | \sigma) = \frac{1}{\sqrt{2\pi}\sigma} \exp\left(-\frac{x^2}{2\sigma^2}\right) \quad (3)$$

15 The estimation problem is nonlinear with five parameters to be determined (i.e., μ , σ , x_0 , α ,
 16 and B). Mathematically, Eq. (1) to (3) can be written as (Kalambet et al., 2011, and references
 17 therein):

$$18 \quad \text{OMI}_{\text{NO}_2, \text{line}}(x | \mu, \sigma, x_0, \alpha, B) = \alpha \cdot \left[\frac{1}{x_0} \exp\left(\frac{\mu}{x_0} + \frac{\sigma^2}{2x_0^2} - \frac{x}{x_0}\right) \Phi\left(\frac{x - \mu}{\sigma} - \frac{\sigma}{x_0}\right) \right] + B \quad (4)$$

19 where x_0 in the exponential function $e(x)$ is the e -folding distance downwind, representing the
 20 length scale of the NO₂ decay; μ is the location of the apparent source relative to the city
 21 center; σ is the standard deviation of the Gaussian function $G(x)$, representing the Gaussian
 22 smoothing length scale; Φ is the cumulative distribution function; B is the offset factor
 23 representing the background NO₂; $f(x)$ is the convolution of $e(x)$ and $G(x)$; and α is the scale
 24 factor of $f(x)$. Since the integration of $f(x)$ equals one, the parameter α physically means the
 25 total number of NO₂ molecules observed near the hotspot, excluding the effect of background
 26 NO₂. α can be converted to mass units, representing the observed OMI NO₂ burden over the
 27 urban areas. Using the mean zonal wind speed w of the NO₂ line density domain, the mean

effective NO₂ lifetime $\tau_{\text{effective}}$ and the mean NO_x emissions E can be calculated from the fitted parameters x_0 and α as

$$\tau_{\text{effective}} = x_0 / w \quad (5)$$

$$E = 1.32 \cdot \alpha / \tau_{\text{effective}} = 1.32 \cdot \alpha \cdot w / x_0 \quad (6)$$

where the factor of 1.32 is the mean NO_x/NO₂ ratio suggested by Beirle et al. (2011).

Fig. 2

We made additional treatments to the OMI NO₂ data when using the EMG method. For urban areas surrounded by significant NO_x emission sources, we discarded the OMI data with certain wind directions in the plume rotation process to limit the influence of surrounding sources on the wind-aligned OMI NO₂ line densities. For example, Washington, DC, is located ~150 km southwest of Philadelphia. On the one hand, the NO₂ of Philadelphia can be transported to Washington, DC, through northeasterly winds and affect the upwind pattern of the OMI line densities of Washington, DC. On the other hand, southwesterly winds can bring the NO₂ plume of Washington, DC, to Philadelphia and affect the downwind pattern of the line densities. In this case, daily OMI NO₂ maps with azimuths of 15° to 105° (i.e., northeasterlies) and 195° to 285° (i.e., southwesterlies) were excluded in the map rotation process. As discussed in detail in Sect. 3.1 and 3.2, the EMG method provides more accurate estimates of NO_x emissions for OMI NO₂ line densities obtained at stronger wind speed conditions (de Foy et al., 2014; Valin et al., 2013; Ialongo et al., 2014), while OMI NO₂ burdens under weak wind conditions correlate better with NO_x emissions. We therefore divided the OMI observations into high and low wind-speed groups (e.g., Fig. 2a and b) and applied the EMG method to both groups. For the high-speed winds group, the OMI-derived NO_x emissions (E) and effective NO₂ lifetimes ($\tau_{\text{effective}}$) were estimated and the wind speeds were set to be above thresholds of 3 to 5 m s⁻¹ depending on the wind fields of each urban area. For the low-speed winds group, the criterion was set to be below 3 m s⁻¹ for all investigated urban areas, and the OMI NO₂ burdens (α) under the slow wind condition were determined. To get reliable estimates through the EMG fit, we further combined all the valid data in three consecutive years in the analysis. Therefore, most results shown in this work are three-year averages or three-year moving trends. For simplicity, we add an asterisk to the middle year to represent the period of three years (e.g., 2006* denotes 2005 to 2007). Through the above treatments, there are at least 30 (up to ~250) valid OMI observations covering the

line density domain of each urban area for both the high- and low-speed winds cases in any three consecutive years during 2005–2014.

We follow the same method used by Beirle et al. (2011) to characterize the uncertainties of the estimates. Unless specified otherwise, the term “uncertainty” in this article refers to one standard deviation (± 1 SD) or the coefficient of variation (CV, SD divided by the mean) expressed as a percentage. Total uncertainties of estimated NO_x emissions are the quadrature sum of the uncertainties in the NO_x/NO_2 ratio (10%), DOMINO v2.0 TVCDs (25%), EMG fitted results, the selected across-wind integration intervals for the line densities (10%), and the wind fields (30%) (Beirle et al., 2011; Boersma et al., 2011). The latter four terms are taken into account for estimated NO_2 burdens, and the latter three are used in calculating the uncertainties of the effective NO_2 lifetimes.

2.5 Bottom-up NO_x emissions and ground-based NO_2 measurements

The OMI-derived NO_x emissions, NO_2 burdens, and their trends for the major U.S. urban areas are compared with both bottom-up NO_x emissions and ground-based NO_2 measurements. The bottom-up NO_x emissions are based on the U.S. EPA’s National Emission Inventory (NEI, <http://www.epa.gov/ttn/chief/eiinformation.html>). For each urban area, we grouped the counties covering the major urban extent and the major OMI NO_2 plume and treated the sum of NEI emissions of these counties as the bottom-up NO_x emissions of this urban area. The counties grouped for each urban area are listed in detail in Table S1 of the Supplement. NO_x emissions at the county level for years 2005, 2008, and 2011 were taken from the NEI directly, and emissions in other years were scaled on the basis of the NEI annual emission trends (<http://www.epa.gov/ttn/chief/trends/index.html>). We did not take into account NO_x emissions of natural sources such as open biomass burning, soil, and lightning, because they are negligible compared to anthropogenic emissions over urban areas in summer.

The ground-based NO_2 measurements are from the U.S. EPA’s Air Quality System (AQS) database (Demerjian, 2000) acquired from the EPA’s AirData website (http://www.epa.gov/airdata/ad_data.html). We only chose monitoring sites spatially located in the NO_2 hotspots of the urban areas and temporally having continuous records in April–September from 2005 to 2014. A total of 110 qualified sites in 35 urban areas were selected and the detailed information is provided in Table S2 of the Supplement. Since the

OMI daily overpass time is at ~13:45 LT (local time), for consistent comparison with the OMI-derived results, we only use hourly NO₂ measurements at 13:00 LT and 14:00 LT in the analysis. The three-year average NO₂ concentration of an urban area is then determined from hourly measurements of all included sites.

3 Results and discussion

3.1 OMI NO₂ TVCDs over the continental U.S. and the wind effects

Figure 1a shows the spatial distribution of average summer OMI NO₂ TVCDs over the U.S. during 2005–2014 with all valid OMI pixel data passing the criteria described in Sect. 2.1. The average TVCDs for the periods of 2005–2007 (i.e., 2006*) and 2012–2014 (i.e., 2013*) are shown in Fig. 3a and b, respectively. Obviously, the NO₂ signals of all selected urban areas are identifiable in these maps because the short lifetime of NO_x in the lower atmosphere makes the NO₂ TVCDs correlate closely with the surface NO_x emissions (e.g., Kim et al., 2006; Martin et al., 2003; Richter et al., 2005). In terms of the OMI-observed NO₂ trend during 2005–2014, a significant reduction in TVCDs up to 50% is observed in visible hotspots and an increase of up to $\sim 0.3 \times 10^{15}$ molecules cm⁻² is observed in rural areas, particularly in the central U.S (Fig. 3c). The hotspot reductions are caused by the technology improvement in the vehicle fleet for the urban areas (Dallmann and Harley, 2010; McDonald et al., 2012) and the mandatory implementation of emission control devices for power plants (Duncan et al., 2013; Kim et al., 2006). The rural increases are believed to be associated with the variations of soil NO_x emissions in recent years (Hudman et al., 2010; Russell et al., 2012). The above NO₂ trends over the U.S. have been more or less reported in a number of previous studies (e.g., Kim et al., 2009; Russell et al., 2012; Tong et al., 2015), although we extended our analysis to the most recent year (i.e., 2014). It should be noted that these previous studies were all based on the satellite maps under all-wind conditions, while we will mainly discuss how the winds affect the satellite-observed NO₂ signals and trends over the urban areas in the following paragraphs.

[Fig. 3](#)

The effect of different wind speeds on the patterns of the OMI-observed NO₂ columns was first shown by Valin et al. (2013) for Riyadh, Saudi Arabia. Here, we take Chicago as an

example to demonstrate this effect. Figures 2a and b display the wind-aligned OMI NO₂ TVCD maps of Chicago when wind speeds are slow ($<3 \text{ m s}^{-1}$) and fast ($>5 \text{ m s}^{-1}$), respectively. The corresponding NO₂ line densities are shown in Fig. 2c. At low wind speeds, NO_x emissions accumulate and stagnate near the urban center, making the peak NO₂ columns about twice those observed at high wind speeds, once the background NO₂ is removed. In contrast, NO₂ plumes can be transported further in high wind-speed conditions, increasing the downwind NO₂ columns at 250 km from the urban center by $\sim 0.9 \times 10^{15} \text{ molecules cm}^{-2}$. These results clearly indicate that the presence of winds, especially high-speed winds, affects the satellite NO₂ observations.

In practice, OMI NO₂ TVCD maps are averaged from valid pixel data with winds at different speeds from different directions (e.g., Fig. 1a, Fig. 3a and b); and, consequently, NO₂ signals near the NO_x emitting sources are smeared spatially. Figure 1b shows the summer mean NO₂ TVCDs over the U.S. during 2005–2014 at wind speeds $<3 \text{ m s}^{-1}$, and the maps for 2005–2007 and 2012–2014 are shown in Fig. 3d and e, respectively. Compared to NO₂ maps under the all-wind condition, NO₂ signals at low wind speeds are obviously higher over the urban areas (as well as in the big isolated power plant areas) and lower in surrounding rural areas (Fig. 1c, Fig. 3g and h); and, consequently, more NO₂ hotspots are visible. In summary, satellite NO₂ maps for low wind-speed conditions highlight the NO_x emission sources. This was also demonstrated in a recent study by Ialongo et al. (2014), who used the OMI pixels with wind speeds $<5 \text{ m s}^{-1}$ to highlight the NO_x signals of three cities in the Baltic Sea region.

The effect of winds on satellite-observed NO₂ columns is not uniform, but depends on the characteristics of the wind fields at each urban location. Figure 4 compares the OMI NO₂ TVCD maps for Chicago and Los Angeles under the all-wind and the weak-wind conditions. Compared to the significant differences in NO₂ columns over Chicago, the discrepancies between the weak-wind and the all-wind conditions over Los Angeles are nearly negligible. This is because the wind fields in these two cities are quite different. According to the ERA-interim reanalysis, the average wind speed of Los Angeles in summer during 2005–2014 was 2.4 m s^{-1} and $\sim 80\%$ of the total valid OMI data were measured under wind speeds of $<3 \text{ m s}^{-1}$. However, the average wind speed was 4.8 m s^{-1} for Chicago and the fraction of valid pixel data with wind speeds $<3 \text{ m s}^{-1}$ was only $\sim 25\%$. Figure 4 also shows that the OMI NO₂ signals observed at low wind speeds are better correlated with the NO_x emissions. Comparing OMI maps under the all-wind condition (Fig. 4a vs. Fig. 4d), Chicago seems to have

1 significantly lower NO_x emissions than Los Angeles. However, on the basis of the NEI,
2 average NO_x emissions from Chicago were about three-quarters of those from Los Angeles
3 during 2005–2014 (Table 1). After removing the pixels with strong winds, the OMI NO₂
4 signals of Chicago and Los Angeles match the amounts of their NEI NO_x emissions much
5 better.

6 [Fig. 4](#)

7 For the reasons discussed above, in contrast to previous studies that use all-wind NO₂ maps,
8 we utilize the OMI data under weak-wind conditions to calculate the satellite-observed NO₂
9 columns, burdens, and trends in these quantities in this work. The threshold of the wind speed
10 was chosen to be 3 m s⁻¹ for all the urban areas to ensure enough valid OMI samples (>30 in
11 three consecutive years). However, we do not discard the OMI data under the strong wind
12 conditions, but use them with the EMG method to obtain “top-down” NO_x emissions (see
13 Sect. 2.4 and the following sections). It should be noted that the presence of the strong winds
14 may also change the observed NO₂ trends. Figure 3i shows the differences in OMI NO₂
15 changes over the U.S. between the weak-wind and the all-wind conditions. Greater NO₂
16 reductions from 2005* to 2013* are observed under the weak-wind condition than under the
17 all-wind condition over a number of cities, including Chicago, Minneapolis, New York, Las
18 Vegas, and Cincinnati. This is possibly related to the non-linearity of the NO_x chemistry. At
19 fast speed winds, the decreased NO₂ level over polluted urban areas may increase the NO_x
20 lifetime so that the same reduction in NO_x emissions would lead to a smaller reduction in
21 observed NO₂ columns compared to the slow wind-speed conditions. For this reason, it is
22 expected that we would derive a higher rate of decline in OMI NO₂ columns over U.S. urban
23 areas than previous studies that have used all-wind OMI data.

24 **3.2 NO_x emissions of U.S. urban areas estimated from the OMI retrievals**

25 As mentioned in Sect. 2.4, we use the EMG method to estimate NO_x emissions from U.S.
26 urban areas. In the original EMG method presented by Beirle et al. (2011), an average wind
27 speed of at least 2 m s⁻¹ was required for a target area to guarantee clear downwind outflow
28 NO₂ patterns. However, Valin et al. (2013) pointed out that the variations of wind speed
29 impact the nonlinear NO_x chemistry, and the NO₂ lifetime (and NO_x emissions) inferred from
30 the average spatial pattern of the NO₂ plume is not necessarily equal to the average lifetime
31 (and emissions). They restricted their analysis to OMI measurements made when winds were

1 fast (i.e., $>6.4 \text{ m s}^{-1}$) because under this condition the downwind decay of NO_2 is dominated
2 by chemical removal, not variability of the winds. In fact, instead of using 6.4 m/s , the same
3 emission estimates would be obtained if they had used the OMI measurements with wind
4 speed $>5 \text{ m s}^{-1}$ (see Figure 4 of Valin et al., 2013). Recently, de Foy et al. (2014) evaluated
5 the EMG method using simulated column densities over an ideal point source with different
6 chemical lifetimes and wind speeds. They found that the EMG method provided fairly robust
7 and accurate emission estimates when wind speeds were $>3 \text{ m s}^{-1}$. Furthermore, the EMG-
8 obtained emissions seemed to be more accurate when wind speeds were higher, especially for
9 case of the chemical lifetime $<12 \text{ h}$ (see Table 2 of de Foy et al., 2014). In this work, we
10 therefore apply the EMG method to the OMI line densities under strong wind-speed
11 conditions to estimate NO_x emissions. The criterion for the wind speed was set to be $>5 \text{ m s}^{-1}$
12 and, if necessary, relaxed to 4 m s^{-1} or 3 m s^{-1} to ensure at least 30 valid OMI samples in
13 three consecutive years.

14 Again, we use the example of Chicago to demonstrate our analytical procedure. Figure 2b
15 shows the wind-aligned OMI NO_2 TVCDs at wind speeds $>5 \text{ m s}^{-1}$ for Chicago during
16 2005–2007 (i.e., the year 2006*). The NO_2 line densities and the corresponding EMG fit are
17 shown in Fig. 2c. Clearly, the EMG fit reproduces the NO_2 pattern along the wind direction
18 very well. The fitted e -folding distance x_0 , background B , and the burden α are 144 km ,
19 $9.83 \times 10^3 \text{ mol km}^{-1}$, and $2.74 \times 10^6 \text{ mol}$, respectively. The average wind speed w of valid OMI
20 pixels over the studied domain is 7.3 m s^{-1} , so that the effective NO_2 lifetime $\tau_{\text{effective}}$ and the
21 NO_x emissions E are determined to be 5.5 h and 30 Mg h^{-1} through Eq. (5) and (6),
22 respectively. We also use the EMG method to fit the NO_2 line densities at wind speeds $<3 \text{ m s}^{-1}$
23 (see Fig. 2 and Sect. 3.1), and the OMI NO_2 burden under the weak-wind condition is
24 estimated to be 98 Mg . The same analysis is conducted for all the three-consecutive-years
25 during 2005–2014 and the three-year moving NO_2 and NO_x trends are summarized in Fig. 5.
26 Results show that the four NO_x -related trends in Chicago correlate with each other very well
27 from 2006* to 2013* ($R>0.89$). The linear annual average decreasing rates (AADR) of the
28 OMI-derived NO_x emissions, the OMI-observed NO_2 burdens at slow winds, the NEI NO_x
29 emission estimates, and the ground-based NO_2 measurements are $-7.8\% \text{ yr}^{-1}$, $-5.7\% \text{ yr}^{-1}$,
30 $-6.6\% \text{ yr}^{-1}$, and $-6.8\% \text{ yr}^{-1}$, respectively. The AADRs of the OMI-observed NO_2 burden is
31 greater than previously reported values of -3.9 to $-5.4\% \text{ yr}^{-1}$ that use the all-wind satellite
32 NO_2 maps (Lamsal et al., 2015; Hilboll et al., 2013; Schneider et al., 2015; Russell et al.,

2012) but close to those of the “top-down” and “bottom-up” emissions as well as surface measurements. This further implies that the presence of strong winds changes the observed NO₂ trends, and trends in NO₂ columns obtained at slow winds may better reflect the real bottom-up NO_x emission trends.

Fig. 5

The above analysis procedure was applied to all 35 selected U.S. urban areas and the average NO_x-related quantities and linear trends for the entire period of 2006*–2013* are summarized in Table 1. We focus on the relationship between NO_x emissions and NO₂ burdens in this section and discuss the trends in the next section. Figures 6a and b show the scatter plots of both the NEI and the OMI-derived NO_x emissions against the OMI NO₂ burdens under slow-wind conditions. Each point in the scatter plots represents a three-year moving average for an urban area. Clearly, there is good agreement between NO_x emissions and OMI NO₂ burdens ($R>0.95$), implying a linear response of the OMI observations to the surface emissions under the weak-wind condition. Generally, urban areas with NO_x emission intensities higher than ~2 Mg h⁻¹ produce statistically significant OMI burdens and can be analyzed using the method described in this work.

Fig. 6

Figure 6c shows the comparison between the OMI-derived and the NEI NO_x emissions for all the selected urban areas. Good agreement was also found between the top-down and the bottom-up emission estimates ($R=0.94$). The slope of the linear fit indicates that the NEI emissions are on average ~6% higher than the OMI-derived ones. Besides the uncertainties of both estimates, any remaining discrepancies can probably be attributed to three factors. First, the NEI NO_x emissions of an urban area are based on the sum of all emissions in counties covering the major urban extent and the major OMI NO₂ plume. Since the outer boundary of the urban area is often somewhat larger than its OMI signals, the NEI values may include more emissions. Second, the OMI-derived NO_x emissions are for the summer half-year, while we did not take into account the seasonality of the NEI emissions. Generally, NO_x emissions of urban areas are lower in summer than in winter because of the relatively low vehicle emissions on warm days and the higher rates of operation of NO_x control devices in some power plants during the ozone season (e.g., Xing et al., 2013; Duncan et al., 2013). Third, a

typical NO_x-to-NO₂ ratio of 1.32 at noon was used in the determination of NO_x emissions, but this scale factor may vary in urban areas depending on the local NO_x chemistry.

In addition to the NO_x emissions, the EMG fits for the OMI line densities at strong winds also yield instantaneous daytime (or, more precisely, 13:00–14:00 LT) lifetimes of NO₂ for selected urban areas. The model evaluation by de Foy et al. (2014) showed that the EMG method provides accurate estimates of the chemical lifetimes (τ_{chemical}) if the plumes are uniformly transported at fast winds (i.e., 5 m s⁻¹). However, influenced by the inaccurate plume rotation and the use of the satellite data at relatively slow wind speeds, they found the resulting lifetimes were always biased low and could not be treated as the true τ_{chemical} . Here, we call this term the effective lifetime ($\tau_{\text{effective}}$), which can be considered as a combination of τ_{chemical} and an extra lifetime term of τ_{extra} related to the influences of plume meandering, grid resolution, and sampling issues (i.e., lifetimes are combined inversely as shown in Eq. (7)) (de Foy et al., 2014, 2015). As summarized in Table 1, the estimated $\tau_{\text{effective}}$ values were in the range of 1.2–6.8 h with a mean of $\sim 3.5 \pm 1.3$ h for all studied urban areas during 2005–2014. They are biased low in comparison to the expected summertime NO₂ τ_{chemical} of ~ 7 h estimated for a broader region in the Eastern United States (Lamsal et al., 2010), confirming the findings by de Foy et al. (2014), but are consistent with previously reported summertime NO₂ lifetimes of 1–7 h examined for plumes over urban areas (Beirle et al., 2011; Dommen et al., 1999; Ialongo et al., 2014; Nunnermacker et al., 1998; Spicer, 1982), power plants (Fioletov et al., 2015; Nunnermacker et al., 2000; Sillman, 2000), and open biomass burning (Alvarado et al., 2010; Mebust et al., 2011).

It should be noted that the slopes of the regression lines of ~ 2.8 h in Fig. 6a and b are also a time term. It can be considered as an average time scale of the OMI-observed NO₂ residency over the emission sources under the slow wind condition. We therefore name it the residence lifetime $\tau_{\text{residence}}$ as suggested by de Foy et al. (2014). In addition to $\tau_{\text{effective}}$, $\tau_{\text{residence}}$ includes the influences of NO₂ physical dispersion in the atmosphere and can be calculated approximately as:

$$\frac{1}{\tau_{\text{residence}}} = \frac{1}{\tau_{\text{dispersion}}} + \frac{1}{\tau_{\text{effective}}} = \frac{1}{\tau_{\text{dispersion}}} + \frac{1}{\tau_{\text{chemical}}} + \frac{1}{\tau_{\text{extra}}} \quad (7)$$

where $\tau_{\text{dispersion}}$ is the physical dispersion time scale. For the slow wind speeds condition, the average dimension of the fitting domain downwind from the urban center was 150 km and the

average wind speed was 2 m s^{-1} . Hence, $\tau_{\text{dispersion}}$ was about 21 h and the average $\tau_{\text{residence}}$ for all the urban areas was estimated to be $\sim 3 \text{ h}$ using Eq. (7), assuming that $\tau_{\text{effective}}$ did not change significantly with wind speed. This $\tau_{\text{residence}}$ estimation is close to the ones derived directly from Fig. 6a and b (i.e., 2.8 h).

3.3 NO₂ and NO_x trends of U.S. urban areas during 2005–2014

The linear trends of the NEI NO_x emissions, OMI-derived NO_x emissions, OMI burdens under the weak-wind condition, and the AQS NO₂ measurements for all 35 selected urban areas from 2006* to 2013* are summarized in Table 1. We have calculated the correlation coefficients of pair-wise trends among these four NO_x-related quantities for each area (see Table 1) and plotted them against the average OMI-observed NO₂ burdens in Fig. 7. Significant reductions in NO₂ and NO_x have occurred in U.S. urban areas. The average percentage reductions among all the studied urban areas from 2006* to 2013* were $-34 \pm 12\%$, $-46 \pm 13\%$, $-45 \pm 15\%$, and $-37 \pm 12\%$ for the NEI NO_x emissions, OMI-derived NO_x emissions, OMI-observed NO₂ burdens, and surface NO₂ measurements, respectively. In general, the time series of the four NO_x-related quantities correlate with each other very well in most of the areas. As shown in Fig. 7 and the last column of Table 1, 20 out of the 35 urban areas have an average correlation coefficient > 0.8 , and only six areas have an average correlation coefficient < 0.7 . The NO_x-related trends are in better agreement with each other for the larger OMI NO₂ hotspots such as New York, Los Angeles, Chicago, Philadelphia, and Washington, DC (mean $R > 0.92$). The poorest correlation among the four NO_x-related series is observed in New Orleans (mean $R = 0.48$), where NO_x emissions are close to the lowest detection limit of the EMG method we suggested in Sect. 3.2 ($\sim 2 \text{ Mg h}^{-1}$).

[Fig. 7](#)

The differences in trends of the four NO_x-related quantities in individual urban areas can be attributed to the following reasons. For the OMI-derived NO₂ and NO_x emissions, we have discussed previously that the selection of the wind speed group and inaccuracy in the wind rotation affects the observed NO₂ trends and the EMG fitted results. Moreover, the EMG method is best suited to point sources; however, urban NO_x emissions are area sources, and the size and shape of the urban area may introduce additional uncertainty to the EMG results. For the NEI emissions, although NO_x emissions from power plants are measured directly using the continuous emissions monitoring system (CEMS), emissions from other sources

1 (e.g., mobile emissions) are still estimated using bottom-up approaches, which have
2 significant uncertainties inherent in the emission factors and the emissions models that are
3 used (USEPA, 1996). For the AQS data, NO₂ measurements at a limited number of
4 monitoring sites can be readily influenced by nearby emission sources and thus may
5 sometimes reflect localized trends rather than urban-scale trends (e.g., Lamsal et al., 2015).
6 Last but not least, there are spatial and temporal mismatches among emissions, OMI
7 observations, and AQS data (e.g., Tong et al., 2015; Bechle et al., 2013). Spatially, OMI
8 provides measurements of tropospheric NO₂ column densities; AQS data are so-called “nose-
9 level” NO₂ concentrations; while emissions are NO_x masses directly discharged into the
10 atmosphere at a variety of heights above the surface. Temporally, the NEI emissions are
11 annual estimates; the OMI data were restricted to the summer half-year and have gone
12 through a series of filtering processes to remove unreliable pixels; and, although we restricted
13 our analysis to the hourly NO₂ measurements close to the OMI overpass time, all AQS
14 measurements at the chosen sites in April–September were used for the trend comparison.

15 Despite the trend discrepancies caused by these various factors in individual urban areas, we
16 expect the trends of the total (or averaged) NO_x emissions, columns, burdens, and
17 concentrations across all areas to be robust and to reflect the urban NO_x situation at the
18 national level. Figure 8 shows the sum of three-year averaged OMI NO₂ columns under the
19 weak-wind speed condition for all urban areas as a function of the distance from the urban
20 centers. Clearly, the sum of OMI signals over the hotspot centers was continuously decreasing
21 during 2006*–2013*. Based on the ratio of 2013* to 2006*, OMI NO₂ columns over U.S.
22 urban areas decreased by 40% with an AADR of $-6.9\% \text{ yr}^{-1}$. The three-year moving trends of
23 the total NEI NO_x emissions, OMI-derived NO_x emissions, OMI-observed NO₂ burdens under
24 slow wind-speed conditions, and the area-weighted average NO₂ concentrations for all areas
25 are shown in Fig. 9. The four NO_x or NO₂ trends are in excellent agreement with each other
26 ($R > 0.99$). From 2006* to 2013*, total NEI NO_x emissions, OMI-derived NO_x emissions,
27 OMI-observed NO₂ burdens, and the average NO₂ concentrations decreased by 36%, 42%,
28 41%, and 37% with AADRs of $-6.2\% \text{ yr}^{-1}$, $-7.4\% \text{ yr}^{-1}$, $-7.3\% \text{ yr}^{-1}$, and $-6.3\% \text{ yr}^{-1}$,
29 respectively (Table 2). The satellite-observed NO₂ rates of decrease obtained in this work are
30 greater than previously reported values. For example, using the OMI BEHR (Berkeley High
31 Resolution) retrievals, Russell et al. (2012) detected consistent decreases in NO₂ columns
32 (AADR of $-6.2\% \text{ yr}^{-1}$) over 47 U.S. cities during 2005–2011; Tong et al. (2015) examined

1 the OMI NO₂ columns over eight large U.S. cities and found an average AADR of $-6.0\% \text{ yr}^{-1}$
2 for 2005–2012; with the newly developed NASA OMI product (version 2.2), Lamsal et al.
3 (2015) quantified the average decreasing rate of NO₂ columns in 20 major U.S. cities from
4 2005 to 2013 to be $-5.8\% \text{ yr}^{-1}$; Schneider et al. (2015) used the data from the SCIAMACHY
5 (Scanning Imaging Absorption Spectrometer for Atmospheric Chartography) instrument
6 onboard the Envisat platform and observed decreasing tropospheric NO₂ columns on the order
7 of $-5.8\% \text{ yr}^{-1}$ over nine large urban agglomerations in the U.S. for the period of 2002–2012.
8 Although these previous studies differ in a number of aspects such as satellite data used (i.e.,
9 instruments/retrievals/products), time period studied (i.e., summer months or all months),
10 urban areas selected, domain size chosen for each area, trend calculation method used, etc.,
11 they derived similar average NO₂ column decrease rates of $-5.8\% \text{ yr}^{-1}$ to $-6.2\% \text{ yr}^{-1}$ for U.S.
12 cities since ~2005. This implies that the differences mentioned above may have minor
13 influence on the overall trend analysis results at the country or regional level. However, we
14 obtain a significantly greater column decrease rate of $-7.3\% \text{ yr}^{-1}$ in this work. As discussed in
15 Sect. 3.1, the fact that all these previous studies used all-wind satellite NO₂ maps while we
16 used weak-wind OMI data is the major reason for such discrepancy.

17 [Fig. 8](#) [Fig. 9](#) [Table 2](#)

18 In previous studies such as Russell et al. (2012), Tong et al. (2015), and Lamsal et al. (2015),
19 OMI NO₂ reduction rates were observed to be moderate ($\sim 7\% \text{ yr}^{-1}$), larger ($\sim 9\% \text{ yr}^{-1}$), and
20 smaller ($\sim 3\% \text{ yr}^{-1}$) during the periods of 2005–2007, 2008–2009, and after 2010,
21 respectively, over the U.S. urban areas. The reason for these changes of pace of the reduction
22 was attributed in these previous studies to the combined effects of the gradually installed NO_x
23 control devices in power plants, transformation to a less-polluting vehicle fleet, the economic
24 recession that happened in 2008, and the slow recovery of the U.S. economy after 2008. In
25 this work, we found similar trends. As shown in Fig. 8 and Fig. 9, the sum of OMI columns,
26 the total NEI NO_x emissions, OMI-derived NO_x emissions, OMI NO₂ burdens, and the
27 average NO₂ concentrations over selected urban areas decreased at rates of -6.8 to $-9.3\% \text{ yr}^{-1}$
28 during 2006*–2010*, and -3.4 to $-4.6\% \text{ yr}^{-1}$ during 2010*–2013* (Table 2). We did not
29 observe a greater decreasing rate during the economic recession period, probably because we
30 used three-year moving trends which smooth the short-term changes. Extrapolating the trends
31 to the years of 2005 and 2014 with AADRs of earlier and later periods, respectively, we

1 estimate that the above five NO_x-related quantities decreased by approximately 47%, 43%,
2 49%, 49%, and 44%, respectively, during the whole period of 2005–2014.

3 Although satellite NO₂ column changes cannot be translated to NO_x emission changes
4 directly, due to the nonlinear feedback of NO_x emissions on NO_x chemistry (Lamsal et al.,
5 2011; Lu and Streets, 2012), we indeed obtained similar reductions in total NO_x emissions
6 and total OMI NO₂ observations over all the selected urban areas in the US. Lamsal et al.
7 (2011) used a dimensionless factor of β to express the relationship between changes in NO_x
8 emissions and changes in NO₂ TVCDs:

$$\beta = \frac{\Delta E / E}{\Delta \text{TVCD} / \text{TVCD}} \quad (8)$$

10 Generally, β is greater than one in clean regions, because increased NO_x emissions under the
11 low NO₂ condition promotes the generation of OH radicals and thus decreases the NO_x
12 lifetime, while β is less than one in polluted regions since an increase in NO_x emissions
13 consumes OH radicals and increases the NO_x lifetime. On the basis of the monthly global
14 gridded β calculated by Lamsal et al. (2011), the average β over the 35 selected urban areas
15 during April–September was 1.03 ± 0.21 (bounding values 0.74–1.52). This result partially
16 explains why we observed similar trends in total NO_x emissions and total OMI NO₂ columns
17 in this work. It should be noted that we only discuss the overall atmospheric characteristics
18 over all urban areas here. Individual areas may have β values significantly greater or smaller
19 than one, reflecting the local sensitivity of changes in OMI NO₂ columns to NO_x emissions.

21 **4 Summary and conclusions**

22 In the present work, we use the satellite observations of NO₂ vertical columns from the OMI
23 instrument to quantify the summer half-year (i.e., April–September) NO_x emissions and
24 emission trends of 35 selected U.S. urban areas during 2005–2014. To refine the analysis, we
25 first explore the impact of winds on the satellite NO₂ observations. Significant differences are
26 found between the OMI NO₂ maps averaged from all valid data and those from data with slow
27 wind speeds only, and such differences are not uniform across all urban areas but depend on
28 local meteorological conditions. Compared to NO₂ maps under all-wind conditions, the
29 satellite-observed NO₂ signals at wind speeds $< 3 \text{ m s}^{-1}$ are significantly higher over the urban
30 areas and lower in surrounding rural areas, and are better correlated to the amounts of surface

1 NO_x emissions. We observe greater NO₂ column reductions over a number of selected cities
2 from 2006* (i.e., 2005–2007) to 2013* (i.e., 2012–2014) under the weak-wind condition than
3 under the all-wind condition, implying that the effect of winds should be taken into account
4 when comparing the trends of NO_x emissions and satellite NO₂ observations.

5 Noticing the importance of wind speed, we divide the OMI observations around each urban
6 area into fast (>3 to 5 m s^{-1}) and slow ($<3 \text{ m s}^{-1}$) wind-speed groups. Daily OMI NO₂ data of
7 each wind-speed group are rotated and oversampled to generate wind-aligned OMI NO₂ maps,
8 the along-wind line densities of which are further fitted by an exponentially-modified
9 Gaussian (EMG) function. For each urban area in any three consecutive years during
10 2005–2014, we derive the corresponding NO_x emissions and effective NO₂ lifetimes from the
11 EMG fits of the fast wind-speed groups and the OMI NO₂ burdens from the slow wind-speed
12 groups. We find good linear agreement ($R>0.93$) among NEI NO_x emissions, OMI-derived
13 NO_x emissions, and OMI NO₂ burdens, implying the possibility of using the satellite NO₂
14 observations under the weak-wind condition to constrain the surface NO_x emissions directly.
15 The simultaneously obtained effective NO₂ lifetimes ($\sim 3.5 \pm 1.3 \text{ h}$) are biased low in
16 comparison to the summertime NO₂ chemical lifetime of $\sim 7 \text{ h}$, reflecting the influences of
17 plume meandering and the coarse sampling resolution on the EMG fitted results.

18 Finally, we quantify the NO_x reductions in selected U.S. urban areas and compare the trends
19 of satellite observations with those of bottom-up emissions and ground-based measurements.
20 We find that the time series of the NO_x-related quantities correlate with each other very well
21 in most U.S. urban areas, especially for large cities. Due to the successful control of NO_x
22 emissions in both the power and transportation sectors, the total NEI NO_x emissions, the total
23 OMI-derived NO_x emissions, the sum of OMI NO₂ columns (under the weak winds
24 condition), the total OMI NO₂ burdens (under the weak winds condition), and the average
25 measured NO₂ concentrations for all U.S. urban areas decreased by 43%, 49%, 47%, 49%,
26 and 44%, respectively, from 2005 to 2014. Reductions of these five NO_x-related quantities
27 were rapid, at rates of -6.8 to $-9.3\% \text{ yr}^{-1}$, before 2010 and slowed down to rates of -3.4 to
28 $-4.9\% \text{ yr}^{-1}$ in recent years. Generally, the annual average rates of decrease of OMI NO₂
29 observations obtained in this work are greater than previously reported values derived from
30 the all-wind satellite maps, further demonstrating the importance of considering winds.

31 We have shown that using the EMG method, the OMI has the capability to estimate NO_x
32 emissions from urban areas directly and constrain their trends with reasonable accuracy.

1 These OMI-derived emissions can provide independent and valuable information to policy
2 makers and researchers in verifying the bottom-up emission estimates and inspecting the
3 effectiveness of emission control measures, especially for areas without complete surface
4 monitoring networks and lacking well-established emission inventories. We also show that a
5 comprehensive and integrated analysis of satellite observations, ground measurements, and
6 bottom-up emissions can provide a better understanding of the true NO_x situation in a given
7 area. Furthermore, the method described in this work can be applied to the near-future
8 satellite missions such as NASA's Tropospheric Emissions: Monitoring of Pollution
9 (TEMPO, Chance et al., 2013) and the European Space Agency's (ESA) Tropospheric Ozone
10 Monitoring Instrument (TROPOMI, Veeffkind et al., 2012). With the improved temporal
11 and/or spatial resolution offered by these missions, the diurnal variations of NO_x emissions
12 and emissions from smaller sources are likely to be able to be inferred.

14 **Supplementary material**

15 Table S1 and Table S2

17 **Acknowledgements**

18 This work was sponsored by the National Aeronautics and Space Administration (NASA) as a
19 part of the Air Quality Applied Sciences Team (AQAST) program, for which we are grateful
20 to the NASA Project Officer John Haynes and the AQAST team leader Daniel Jacob. We
21 acknowledge the free use of tropospheric NO₂ column data from the OMI sensor from
22 www.temis.nl. Argonne National Laboratory is operated by UChicago Argonne, LLC, under
23 Contract No. DE-AC02-06CH11357 with the U.S. Department of Energy.

25 **References**

26 Alvarado, M. J., Logan, J. A., Mao, J., Apel, E., Riemer, D., Blake, D., Cohen, R. C., Min, K.
27 E., Perring, A. E., Browne, E. C., Wooldridge, P. J., Diskin, G. S., Sachse, G. W.,
28 Fuelberg, H., Sessions, W. R., Harrigan, D. L., Huey, G., Liao, J., Case-Hanks, A.,
29 Jimenez, J. L., Cubison, M. J., Vay, S. A., Weinheimer, A. J., Knapp, D. J., Montzka, D.
30 D., Flocke, F. M., Pollack, I. B., Wennberg, P. O., Kurten, A., Crounse, J., St Clair, J. M.,

- 1 Wisthaler, A., Mikoviny, T., Yantosca, R. M., Carouge, C. C., and Le Sager, P.: Nitrogen
2 oxides and PAN in plumes from boreal fires during ARCTAS-B and their impact on
3 ozone: an integrated analysis of aircraft and satellite observations, *Atmos. Chem. Phys.*,
4 10, 9739-9760, 2010.
- 5 Bechle, M. J., Millet, D. B., and Marshall, J. D.: Remote sensing of exposure to NO₂: satellite
6 versus ground-based measurement in a large urban, *Atmos. Environ.*, 69, 345-353, 2013.
- 7 Beirle, S., Platt, U., von Glasow, R., Wenig, M., and Wagner, T.: Estimate of nitrogen oxide
8 emissions from shipping by satellite remote sensing, *Geophys. Res. Lett.*, 31, L18102,
9 doi:10.1029/2004gl020312, 2004.
- 10 Beirle, S., Boersma, K. F., Platt, U., Lawrence, M. G., and Wagner, T.: Megacity emissions
11 and lifetimes of nitrogen oxides probed from space, *Science*, 333, 1737-1739, 2011.
- 12 Beirle, S., Hormann, C., de Vries, M. P., Dorner, S., Kern, C., and Wagner, T.: Estimating the
13 volcanic emission rate and atmospheric lifetime of SO₂ from space: a case study for
14 Kilauea volcano, Hawai'i, *Atmos. Chem. Phys.*, 14, 8309-8322, 2014.
- 15 Boersma, K. F., Eskes, H. J., Meijer, E. W., and Kelder, H. M.: Estimates of lightning NO_x
16 production from GOME satellite observations, *Atmos. Chem. Phys.*, 5, 2311-2331, 2005.
- 17 Boersma, K. F., Eskes, H. J., Veefkind, J. P., Brinksma, E. J., van der A, R. J., Sneep, M., van
18 den Oord, G. H. J., Levelt, P. F., Stammes, P., Gleason, J. F., and Bucsela, E. J.: Near-real
19 time retrieval of tropospheric NO₂ from OMI, *Atmos. Chem. Phys.*, 7, 2103-2118, 2007.
- 20 Boersma, K. F., Eskes, H. J., Dirksen, R. J., van der A, R. J., Veefkind, J. P., Stammes, P.,
21 Huijnen, V., Kleipool, Q. L., Sneep, M., Claas, J., Leitao, J., Richter, A., Zhou, Y., and
22 Brunner, D.: An improved tropospheric NO₂ column retrieval algorithm for the Ozone
23 Monitoring Instrument, *Atmos. Meas. Tech.*, 4, 1905-1928, 2011.
- 24 Carn, S. A., Krotkov, N. A., Yang, K., and Krueger, A. J.: Measuring global volcanic
25 degassing with the Ozone Monitoring Instrument (OMI), in: *Remote Sensing of*
26 *Volcanoes and Volcanic Processes: Integrating Observation and Modeling*, edited by:
27 Pyle, D. M., Mather, T. A., and Biggs, J., Geological Society, Special Publications, 380,
28 London, 229-257, 2013.
- 29 Chance, K., Liu, X., Suleiman, R. M., Flittner, D. E., Al-Saadi, J., and Janz, S. J.:
30 Tropospheric emissions: monitoring of pollution (TEMPO), in: *Proc. SPIE 8866, Earth*

- 1 Observing Systems XVIII, San Diego, California, USA, August 25, 2013,
2 doi:10.1117/12.2024479, 2013.
- 3 Dallmann, T. R., and Harley, R. A.: Evaluation of mobile source emission trends in the
4 United States, *J. Geophys. Res.*, 115, D14305, doi:10.1029/2010jd013862, 2010.
- 5 de Foy, B., Krotkov, N. A., Bei, N., Herndon, S. C., Huey, L. G., Martinez, A. P., Ruiz-
6 Suarez, L. G., Wood, E. C., Zavala, M., and Molina, L. T.: Hit from both sides: tracking
7 industrial and volcanic plumes in Mexico City with surface measurements and OMI SO₂
8 retrievals during the MILAGRO field campaign, *Atmos. Chem. Phys.*, 9, 9599-9617,
9 2009.
- 10 de Foy, B., Wilkins, J. L., Lu, Z., Streets, D. G., and Duncan, B. N.: Model evaluation of
11 methods for estimating surface emissions and chemical lifetimes from satellite data,
12 *Atmos. Environ.*, 98, 66-77, 2014.
- 13 de Foy, B., Lu, Z., Streets, D. G., Lamsal, L. N., and Duncan, B. N.: Estimates of power plant
14 NO_x emissions and lifetimes from OMI NO₂ satellite retrievals, *Atmos. Environ.*, 116, 1-
15 11, 2015.
- 16 Dee, D. P., Uppala, S. M., Simmons, A. J., Berrisford, P., Poli, P., Kobayashi, S., Andrae, U.,
17 Balmaseda, M. A., Balsamo, G., Bauer, P., Bechtold, P., Beljaars, A. C. M., van de Berg,
18 L., Bidlot, J., Bormann, N., Delsol, C., Dragani, R., Fuentes, M., Geer, A. J., Haimberger,
19 L., Healy, S. B., Hersbach, H., Holm, E. V., Isaksen, L., Kallberg, P., Kohler, M.,
20 Matricardi, M., McNally, A. P., Monge-Sanz, B. M., Morcrette, J. J., Park, B. K., Peubey,
21 C., de Rosnay, P., Tavolato, C., Thepaut, J. N., and Vitart, F.: The ERA-Interim
22 reanalysis: configuration and performance of the data assimilation system, *Q. J. Roy.
23 Meteor. Soc.*, 137, 553-597, 2011.
- 24 Demerjian, K. L.: A review of national monitoring networks in North America, *Atmos.
25 Environ.*, 34, 1861-1884, 2000.
- 26 Dommen, J., Prevot, A. S. H., Hering, A. M., Staffelbach, T., Kok, G. L., and Schillawski, R.
27 D.: Photochemical production and aging of an urban air mass, *J. Geophys. Res.*, 104,
28 5493-5506, 1999.
- 29 Duncan, B. N., Yoshida, Y., de Foy, B., Lamsal, L. N., Streets, D. G., Lu, Z., Pickering, K.
30 E., and Krotkov, N. A.: The observed response of Ozone Monitoring Instrument (OMI)

1 NO₂ columns to NO_x emission controls on power plants in the United States: 2005-2011,
2 Atmos. Environ., 81, 102-111, 2013.

3 Fioletov, V. E., McLinden, C. A., Krotkov, N., Moran, M. D., and Yang, K.: Estimation of
4 SO₂ emissions using OMI retrievals, Geophys. Res. Lett., 38, L21811,
5 doi:10.1029/2011gl049402, 2011.

6 Fioletov, V. E., McLinden, C. A., Krotkov, N., Yang, K., Loyola, D. G., Valks, P., Theys, N.,
7 Van Roozendaal, M., Nowlan, C. R., Chance, K., Liu, X., Lee, C., and Martin, R. V.:
8 Application of OMI, SCIAMACHY, and GOME-2 satellite SO₂ retrievals for detection of
9 large emission sources, J. Geophys. Res., 118, 11399-11418, 2013.

10 Fioletov, V. E., McLinden, C. A., Krotkov, N., and Li, C.: Lifetimes and emissions of SO₂
11 from point sources estimated from OMI, Geophys. Res. Lett., 42, 1969-1976, 2015.

12 Hilboll, A., Richter, A., and Burrows, J. P.: Long-term changes of tropospheric NO₂ over
13 megacities derived from multiple satellite instruments, Atmos. Chem. Phys., 13, 4145-
14 4169, 2013.

15 Hudman, R. C., Russell, A. R., Valin, L. C., and Cohen, R. C.: Interannual variability in soil
16 nitric oxide emissions over the United States as viewed from space, Atmos. Chem. Phys.,
17 10, 9943-9952, 2010.

18 Ialongo, I., Hakkarainen, J., Hyttinen, N., Jalkanen, J. P., Johansson, L., Boersma, K. F.,
19 Krotkov, N., and Tamminen, J.: Characterization of OMI tropospheric NO₂ over the Baltic
20 Sea region, Atmos. Chem. Phys., 14, 7795-7805, 2014.

21 Jaeglé, L., Steinberger, L., Martin, R. V., and Chance, K.: Global partitioning of NO_x sources
22 using satellite observations: relative roles of fossil fuel combustion, biomass burning and
23 soil emissions, Faraday Discuss., 130, 407-423, 2005.

24 Kalambet, Y., Kozmin, Y., Mikhailova, K., Nagaev, I., and Tikhonov, P.: Reconstruction of
25 chromatographic peaks using the exponentially modified Gaussian function, J.
26 Chemometr., 25, 352-356, 2011.

27 Kim, S. W., Heckel, A., McKeen, S. A., Frost, G. J., Hsie, E. Y., Trainer, M. K., Richter, A.,
28 Burrows, J. P., Peckham, S. E., and Grell, G. A.: Satellite-observed US power plant NO_x
29 emission reductions and their impact on air quality, Geophys. Res. Lett., 33, L22812,
30 doi:10.1029/2006gl027749, 2006.

1 Kim, S. W., Heckel, A., Frost, G. J., Richter, A., Gleason, J., Burrows, J. P., McKeen, S.,
2 Hsie, E. Y., Granier, C., and Trainer, M.: NO₂ columns in the western United States
3 observed from space and simulated by a regional chemistry model and their implications
4 for NO_x emissions, *J. Geophys. Res.*, 114, D11301, doi:10.1029/2008jd011343, 2009.

5 Krotkov, N. A., Schoeberl, M. R., Morris, G. A., Carn, S., and Yang, K.: Dispersion and
6 lifetime of the SO₂ cloud from the August 2008 Kasatochi eruption, *J. Geophys. Res.*,
7 115, D00120, doi:10.1029/2010jd013984, 2010.

8 Kunhikrishnan, T., Lawrence, M. G., von Kuhlmann, R., Richter, A., Ladstatter-
9 Weissenmayer, A., and Burrows, J. P.: Analysis of tropospheric NO_x over Asia using the
10 model of atmospheric transport and chemistry (MATCH-MPIC) and GOME-satellite
11 observations, *Atmos. Environ.*, 38, 581-596, 2004.

12 Lamsal, L. N., Martin, R. V., van Donkelaar, A., Celarier, E. A., Bucsela, E. J., Boersma, K.
13 F., Dirksen, R., Luo, C., and Wang, Y.: Indirect validation of tropospheric nitrogen
14 dioxide retrieved from the OMI satellite instrument: insight into the seasonal variation of
15 nitrogen oxides at northern midlatitudes, *J. Geophys. Res.*, 115, D05302,
16 doi:10.1029/2009jd013351, 2010.

17 Lamsal, L. N., Martin, R. V., Padmanabhan, A., van Donkelaar, A., Zhang, Q., Sioris, C. E.,
18 Chance, K., Kurosu, T. P., and Newchurch, M. J.: Application of satellite observations for
19 timely updates to global anthropogenic NO_x emission inventories, *Geophys. Res. Lett.*,
20 38, L05810, doi:10.1029/2010gl046476, 2011.

21 Lamsal, L. N., Duncan, B. N., Yoshida, Y., Krotkov, N. A., Pickering, K. E., Streets, D. G.,
22 and Lu, Z.: U.S. NO₂ trends (2005-2013): EPA Air Quality System (AQS) data versus
23 improved observations from the Ozone Monitoring Instrument (OMI), *Atmos. Environ.*,
24 110, 130-143, 2015.

25 Leue, C., Wenig, M., Wagner, T., Klimm, O., Platt, U., and Jahne, B.: Quantitative analysis of
26 NO_x emissions from Global Ozone Monitoring Experiment satellite image sequences, *J.*
27 *Geophys. Res.*, 106, 5493-5505, 2001.

28 Levelt, P. F., Van den Oord, G. H. J., Dobber, M. R., Malkki, A., Visser, H., de Vries, J.,
29 Stammes, P., Lundell, J. O. V., and Saari, H.: The Ozone Monitoring Instrument, *IEEE T.*
30 *Geosci. Remote*, 44, 1093-1101, 2006.

1 Lu, Z., and Streets, D. G.: Increase in NO_x emissions from Indian thermal power plants during
2 1996-2010: unit-based inventories and multisatellite observations, *Environ. Sci. Technol.*,
3 46, 7463-7470, 2012.

4 Lu, Z., Streets, D. G., de Foy, B., and Krotkov, N. A.: Ozone Monitoring Instrument
5 observations of interannual increases in SO₂ emissions from Indian coal-fired power
6 plants during 2005-2012, *Environ. Sci. Technol.*, 47, 13993-14000, 2013.

7 Martin, R. V., Jacob, D. J., Chance, K., Kurosu, T. P., Palmer, P. I., and Evans, M. J.: Global
8 inventory of nitrogen oxide emissions constrained by space-based observations of NO₂
9 columns, *J. Geophys. Res.*, 108, D17, 4537, doi:10.1029/2003jd003453, 2003.

10 Martin, R. V.: Satellite remote sensing of surface air quality, *Atmos. Environ.*, 42, 7823-7843,
11 2008.

12 McDonald, B. C., Dallmann, T. R., Martin, E. W., and Harley, R. A.: Long-term trends in
13 nitrogen oxide emissions from motor vehicles at national, state, and air basin scales, *J.*
14 *Geophys. Res.*, 117, D00v18, doi:10.1029/2012jd018304, 2012.

15 Mebust, A. K., Russell, A. R., Hudman, R. C., Valin, L. C., and Cohen, R. C.:
16 Characterization of wildfire NO_x emissions using MODIS fire radiative power and OMI
17 tropospheric NO₂ columns, *Atmos. Chem. Phys.*, 11, 5839-5851, 2011.

18 Nunnermacker, L. J., Imre, D., Daum, P. H., Kleinman, L., Lee, Y. N., Lee, J. H., Springston,
19 S. R., Newman, L., Weinstein-Lloyd, J., Luke, W. T., Banta, R., Alvarez, R., Senff, C.,
20 Sillman, S., Holdren, M., Keigley, G. W., and Zhou, X.: Characterization of the Nashville
21 urban plume on July 3 and July 18, 1995, *J. Geophys. Res.*, 103, 28129-28148, 1998.

22 Nunnermacker, L. J., Kleinman, L. I., Imre, D., Daum, P. H., Lee, Y. N., Lee, J. H.,
23 Springston, S. R., Newman, L., and Gillani, N.: NO_y lifetimes and O₃ production
24 efficiencies in urban and power plant plumes: analysis of field data, *J. Geophys. Res.*, 105,
25 9165-9176, 2000.

26 Richter, A., Burrows, J. P., Nuss, H., Granier, C., and Niemeier, U.: Increase in tropospheric
27 nitrogen dioxide over China observed from space, *Nature*, 437, 129-132, 2005.

28 Russell, A. R., Valin, L. C., Bucsela, E. J., Wenig, M. O., and Cohen, R. C.: Space-based
29 constraints on spatial and temporal patterns of NO_x emissions in California, 2005-2008,
30 *Environ. Sci. Technol.*, 44, 3608-3615, 2010.

1 Russell, A. R., Valin, L. C., and Cohen, R. C.: Trends in OMI NO₂ observations over the
2 United States: effects of emission control technology and the economic recession, *Atmos.*
3 *Chem. Phys.*, 12, 12197-12209, 2012.

4 Schneider, P., Lahoz, W. A., and van der A, R.: Recent satellite-based trends of tropospheric
5 nitrogen dioxide over large urban agglomerations worldwide, *Atmos. Chem. Phys.*, 15,
6 1205-1220, 2015.

7 Sillman, S.: Ozone production efficiency and loss of NO_x in power plant plumes:
8 photochemical model and interpretation of measurements in Tennessee, *J. Geophys. Res.*,
9 105, 9189-9202, 2000.

10 Spicer, C. W.: Nitrogen-oxide reactions in the urban plume of Boston, *Science*, 215, 1095-
11 1097, 1982.

12 Streets, D. G., Canty, T., Carmichael, G. R., de Foy, B., Dickerson, R. R., Duncan, B. N.,
13 Edwards, D. P., Haynes, J. A., Henze, D. K., Houyoux, M. R., Jacobi, D. J., Krotkov, N.
14 A., Lamsal, L. N., Liu, Y., Lu, Z., Martini, R. V., Pfister, G. G., Pinder, R. W., Salawitch,
15 R. J., and Wechti, K. J.: Emissions estimation from satellite retrievals: a review of current
16 capability, *Atmos. Environ.*, 77, 1011-1042, 2013.

17 Streets, D. G., de Foy, B., Duncan, B. N., Lamsal, L. N., Li, C., and Lu, Z.: Using satellite
18 observations to measure power plant emissions and their trends, *EM Magazine*, 64, 16-21,
19 2014.

20 Theys, N., Campion, R., Clarisse, L., Brenot, H., van Gent, J., Dils, B., Corradini, S.,
21 Merucci, L., Coheur, P. F., Van Roozendael, M., Hurtmans, D., Clerbaux, C., Tait, S., and
22 Ferrucci, F.: Volcanic SO₂ fluxes derived from satellite data: a survey using OMI,
23 GOME-2, IASI and MODIS, *Atmos. Chem. Phys.*, 13, 5945-5968, 2013.

24 Tong, D. Q., Lamsal, L. N., Pan, L., Ding, C., Kim, H., Lee, P., Chai, T., Pickering, K. E., and
25 Stajner, I.: Long-term NO_x trends over large cities in the United States during the Great
26 Recession: comparison of satellite retrievals, ground observations, and
27 emission inventories, *Atmos. Environ.*, 107, 70-84, 2015.

28 USEPA: Evaluating the uncertainty of emission estimates, Volume VI, Chapter 4, Research
29 Triangle Park, North Carolina, USA, 1996.

- 1 Valin, L. C., Russell, A. R., and Cohen, R. C.: Variations of OH radical in an urban plume
2 inferred from NO₂ column measurements, *Geophys. Res. Lett.*, 40, 1856-1860, 2013.
- 3 van der A, R. J., Eskes, H. J., Boersma, K. F., van Noije, T. P. C., Van Roozendaal, M., De
4 Smedt, I., Peters, D. H. M. U., and Meijer, E. W.: Trends, seasonal variability and
5 dominant NO_x source derived from a ten year record of NO₂ measured from space, *J.*
6 *Geophys. Res.*, 113, D04302, doi:10.1029/2007jd009021, 2008.
- 7 Veeffkind, J. P., Aben, I., McMullan, K., Forster, H., de Vries, J., Otter, G., Claas, J., Eskes,
8 H. J., de Haan, J. F., Kleipool, Q., van Weele, M., Hasekamp, O., Hoogeveen, R.,
9 Landgraf, J., Snel, R., Tol, P., Ingmann, P., Voors, R., Kruizinga, B., Vink, R., Visser, H.,
10 and Levelt, P. F.: TROPOMI on the ESA Sentinel-5 Precursor: a GMES mission for
11 global observations of the atmospheric composition for climate, air quality and ozone
12 layer applications, *Remote Sens. Environ.*, 120, 70-83, 2012.
- 13 Wang, S. W., Streets, D. G., Zhang, Q. A., He, K. B., Chen, D., Kang, S. C., Lu, Z., and
14 Wang, Y. X.: Satellite detection and model verification of NO_x emissions from power
15 plants in Northern China, *Environ. Res. Lett.*, 5, 044007, doi:10.1088/1748-
16 9326/5/4/044007, 2010.
- 17 Wang, S. W., Zhang, Q., Streets, D. G., He, K. B., Martin, R. V., Lamsal, L. N., Chen, D.,
18 Lei, Y., and Lu, Z.: Growth in NO_x emissions from power plants in China: bottom-up
19 estimates and satellite observations, *Atmos. Chem. Phys.*, 12, 4429-4447, 2012.
- 20 Xing, J., Pleim, J., Mathur, R., Pouliot, G., Hogrefe, C., Gan, C. M., and Wei, C.: Historical
21 gaseous and primary aerosol emissions in the United States from 1990 to 2010, *Atmos.*
22 *Chem. Phys.*, 13, 7531-7549, 2013.
- 23 Zhang, Q., Streets, D. G., and He, K. B.: Satellite observations of recent power plant
24 construction in Inner Mongolia, China, *Geophys. Res. Lett.*, 36, L15809,
25 doi:10.1029/2009gl038984, 2009.

26

27

Figure captions

Fig. 1. Average summer half-year (i.e., April to September) OMI NO₂ TVCDs over the continental U.S. during 2005–2014: (a) all valid data were used, (b) only valid data with wind speeds $<3 \text{ m s}^{-1}$ were used, and (c) the difference between (b) and (a). Squares in (a) indicate the urban areas selected in this work.

Fig. 2. Wind-aligned OMI NO₂ TVCD maps at wind speeds (a) $<3 \text{ m s}^{-1}$ and (b) $>5 \text{ m s}^{-1}$ for Chicago in summer months (i.e., April to September) during 2005–2007. (c) OMI NO₂ line densities of (a) and (b) and the corresponding EMG fits. Line densities are from the integration of the NO₂ data in the across-wind direction.

Fig. 3. Average summer half-year (i.e., April to September) OMI NO₂ TVCDs over the continental U.S. for (a, d) 2006* (i.e., 2005 to 2007) and (b, e) 2013* (i.e., 2012 to 2014): (a, b) all valid data were used, (d, e) only valid data with wind speeds $<3 \text{ m s}^{-1}$ were used. The right column shows the differences in maps between the middle and the left column. The bottom row shows the differences in maps between the middle and the top row.

Fig. 4. Average summer half-year (i.e., April to September) OMI NO₂ TVCDs over (a, b) Chicago and (d, e) Los Angeles during 2005–2014: (a, d) all valid data were used, (b, e) only valid data with wind speeds $<3 \text{ m s}^{-1}$ were used, and (c, f) the difference between the middle and the left column.

Fig. 5. Interannual trends of NEI NO_x emissions, the OMI-derived summertime (April to September) NO_x emissions, the OMI-observed summertime NO₂ burdens at low ($<3 \text{ m s}^{-1}$) speed winds condition, and the average summertime NO₂ concentrations at 13:00–14:00 LT in Chicago during 2006*–2013*. Error bars express the ± 1 SD of the annually estimated results. *R* values shown are the correlation coefficients with the OMI-observed NO₂ burdens.

Fig. 6. Scatter plots of (a) OMI-observed NO₂ burdens at low ($<3 \text{ m s}^{-1}$) speed winds condition against NEI NO_x emissions, (b) OMI-observed NO₂ burdens against OMI-derived NO_x emissions, and (c) OMI-derived NO_x emissions against NEI NO_x emissions for 35 selected U.S. urban areas during 2005–2014. Each point represents a three-year result for an urban area. Error bars express the ± 1 SD

1 uncertainties. Uncertainties of NEI emissions are set to be 50% according to the
2 expert judgment. The inset figures are the zoomed views of points with emissions
3 $<20 \text{ Mg h}^{-1}$.

4 Fig. 7. Correlation coefficients of pair-wise trends among the NEI NO_x emissions, the
5 OMI-derived NO_x emissions, the OMI NO_2 burdens at wind speeds $<3 \text{ m s}^{-1}$, and
6 the AQS NO_2 measurements against the mean OMI NO_2 burdens under the weak-
7 wind speed condition ($<3 \text{ m s}^{-1}$) for all selected urban areas during 2006*–2013*.
8 Each large gray circle represents the average of the six correlation coefficients for
9 an urban area.

10 Fig. 8. The sum of three-year averaged OMI NO_2 TVCDs under the weak-wind speed
11 condition for 35 selected U.S. urban areas as a function of the distance from the
12 urban centers during 2006* to 2013*. The background NO_2 of urban areas was
13 removed. Error bars express the 95% confidence intervals of the mean. The ratios
14 of 2007* to 2006*, 2010* to 2006*, and 2013* to 2006* are shown at the top.

15 Fig. 9. Three-year moving trends of the total NEI NO_x emissions, the total OMI-derived
16 NO_x emissions, the total OMI-observed NO_2 burdens under the weak-wind speed
17 condition, and the area-weighted average AQS surface NO_2 measurements for all
18 selected urban areas during 2006*–2013*. Error bars express the ± 1 SD of the
19 estimates. R values shown are the correlation coefficients with the OMI-observed
20 NO_2 burdens.

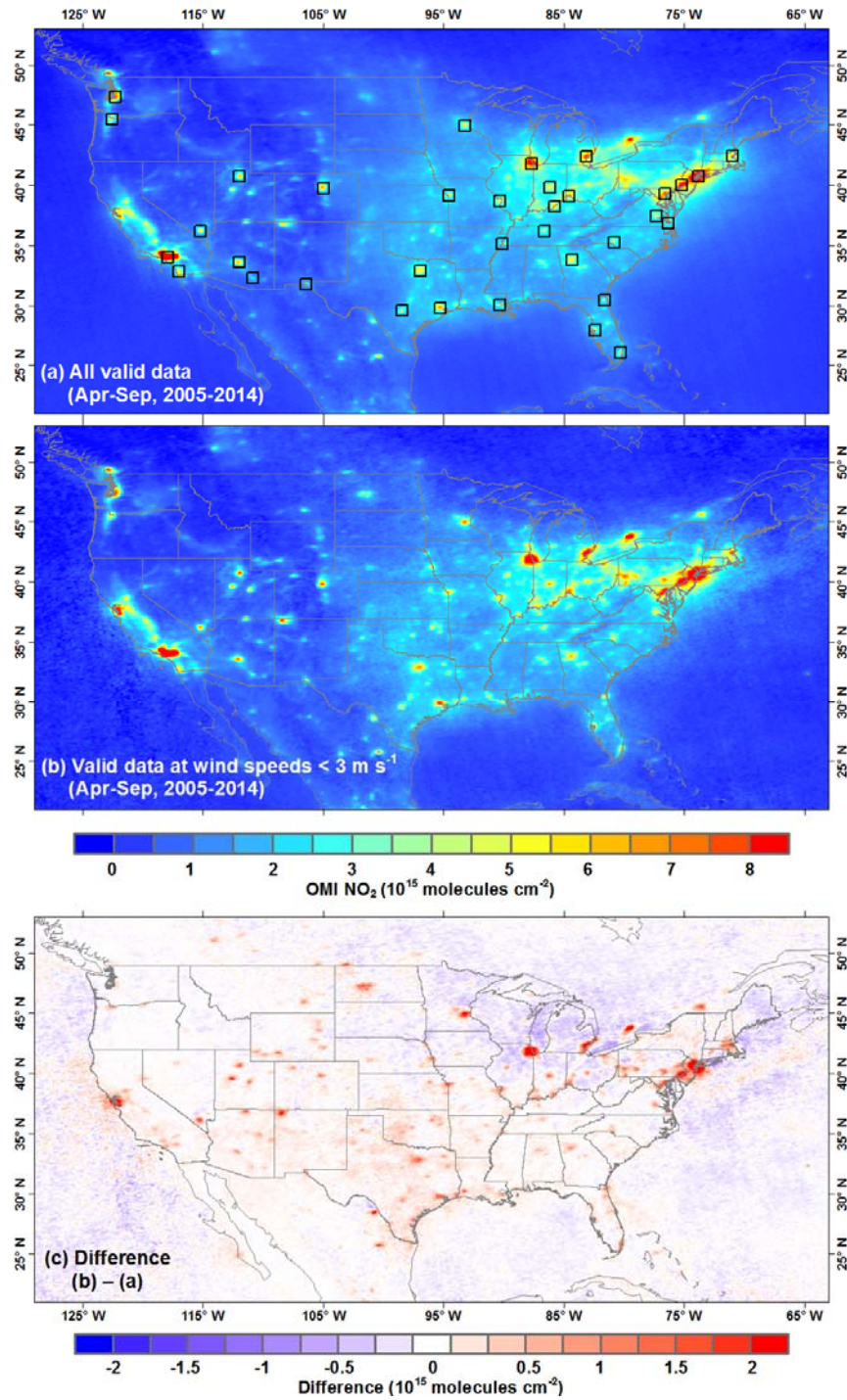


Fig. 1. Average summer half-year (i.e., April to September) OMI NO₂ TVCDs over the continental U.S. during 2005–2014: (a) all valid data were used, (b) only valid data with wind speeds <3 m s⁻¹ were used, and (c) the difference between (b) and (a). Squares in (a) indicate the urban areas selected in this work.

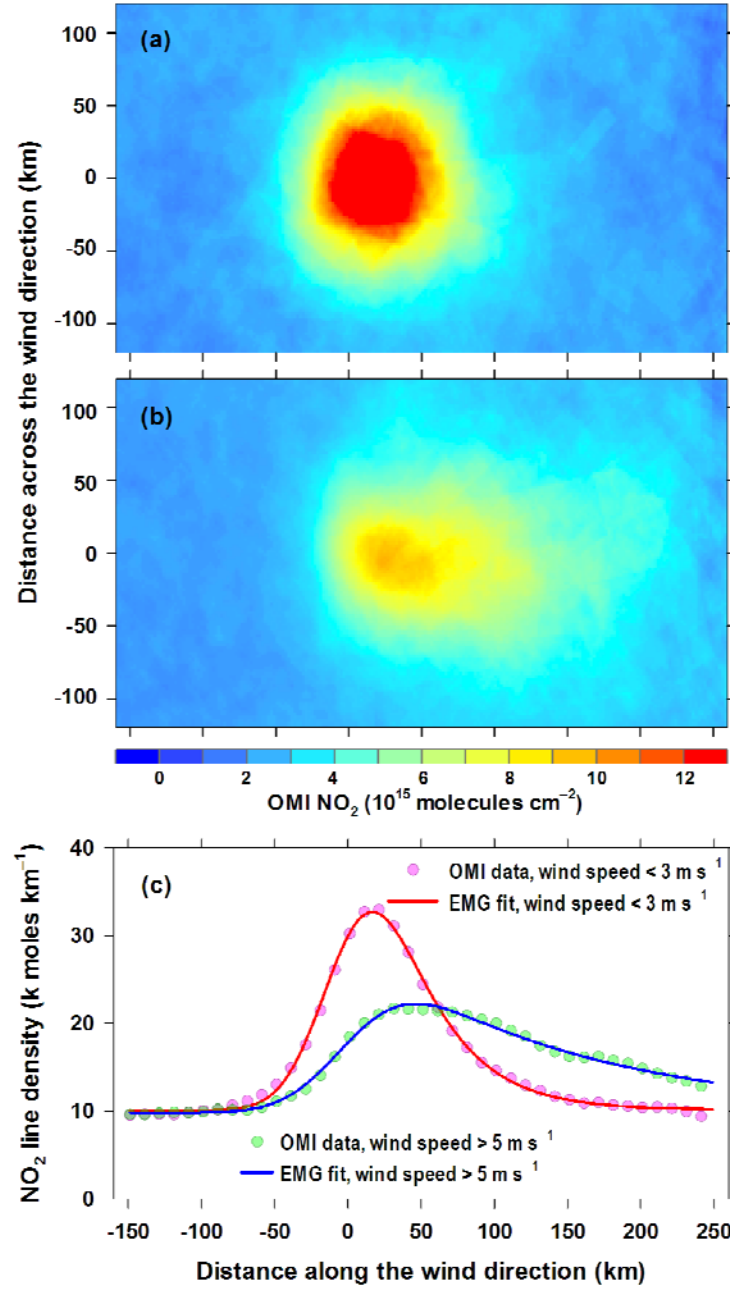


Fig. 2. Wind-aligned OMI NO₂ TVCD maps at wind speeds (a) <3 m s⁻¹ and (b) >5 m s⁻¹ for Chicago in summer months (i.e., April to September) during 2005–2007. (c) OMI NO₂ line densities of (a) and (b) and the corresponding EMG fits. Line densities are from the integration of the NO₂ data in the across-wind direction.

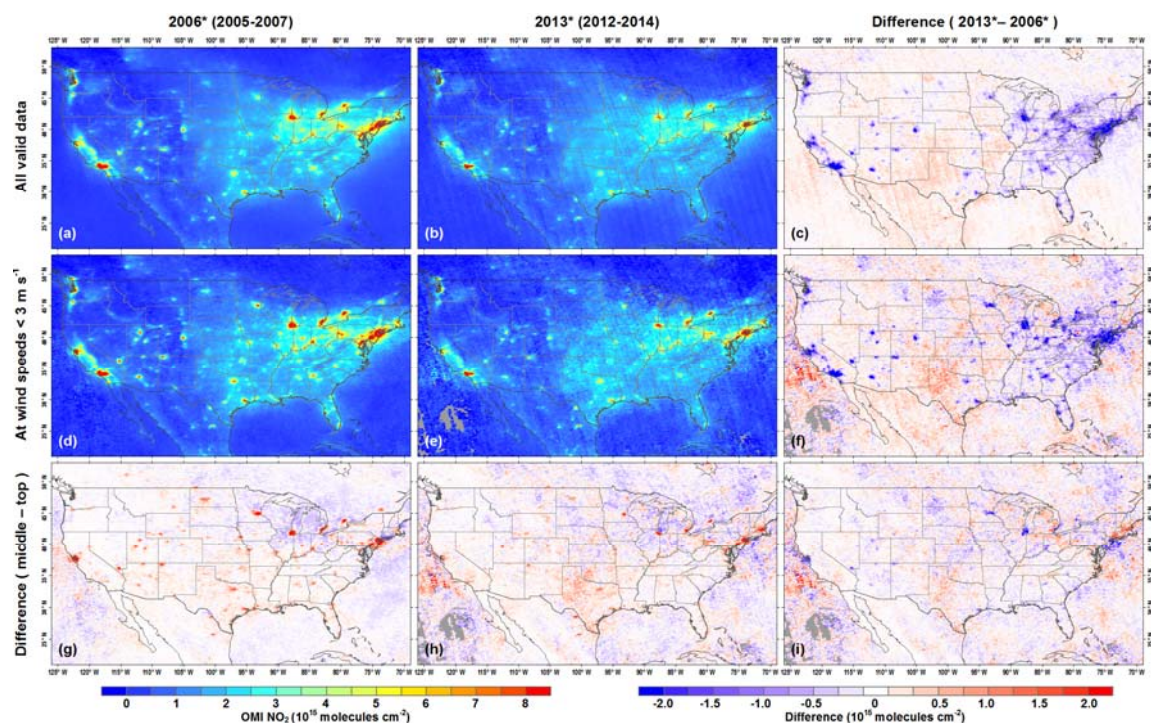


Fig. 3. Average summer half-year (i.e., April to September) OMI NO₂ TVCDs over the continental U.S. for (a, d) 2006* (i.e., 2005 to 2007) and (b, e) 2013* (i.e., 2012 to 2014): (a, b) all valid data were used, (d, e) only valid data with wind speeds <3 m s⁻¹ were used. The right column shows the differences in maps between the middle and the left column. The bottom row shows the differences in maps between the middle and the top row.

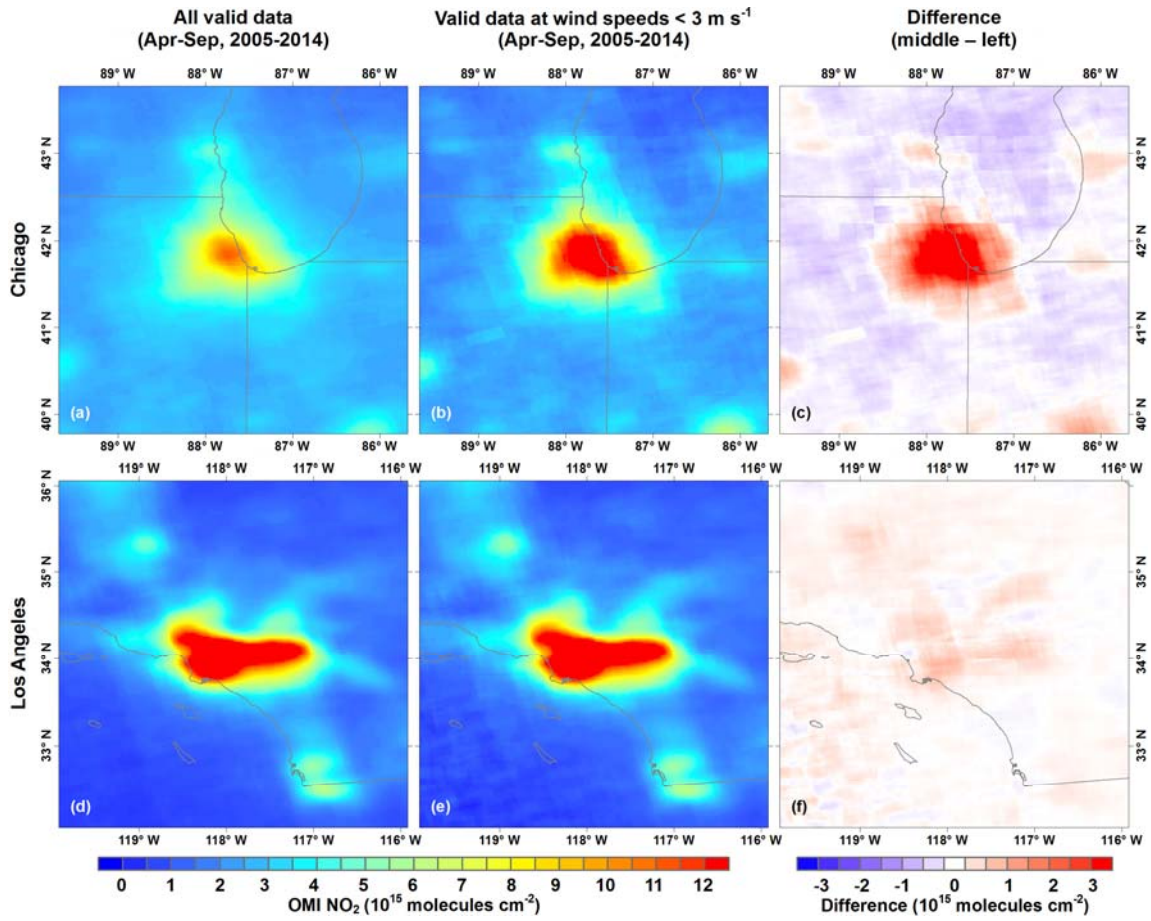


Fig. 4. Average summer half-year (i.e., April to September) OMI NO₂ TVCDs over (a, b) Chicago and (d, e) Los Angeles during 2005–2014: (a, d) all valid data were used, (b, e) only valid data with wind speeds <3 m s⁻¹ were used, and (c, f) the difference between the middle and the left column.

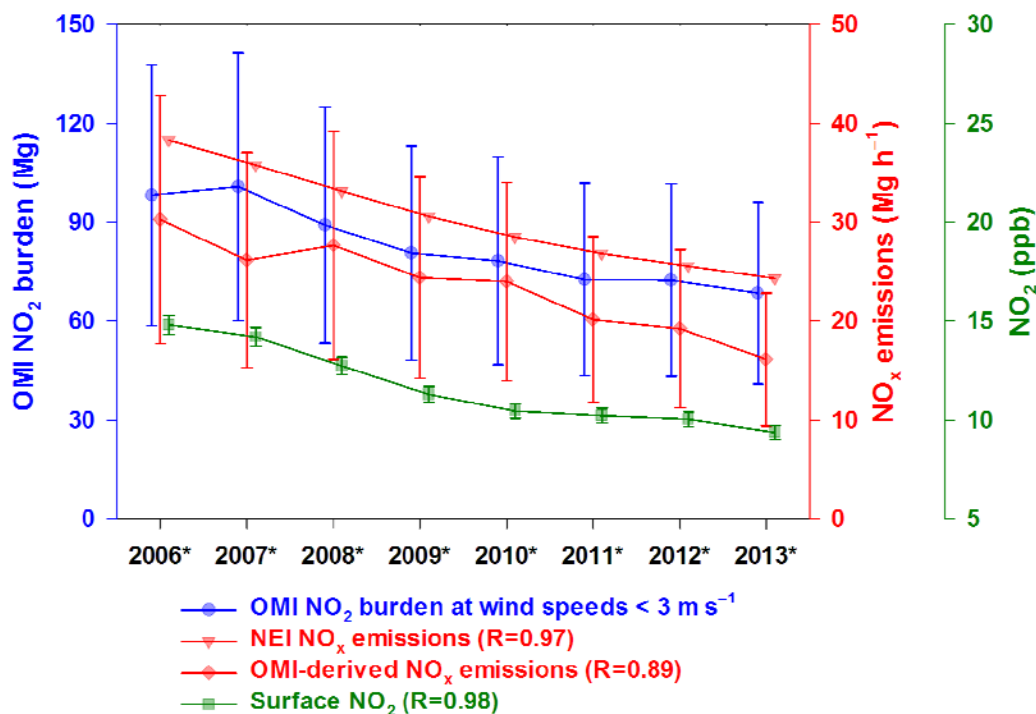


Fig. 5. Interannual trends of NEI NO_x emissions, the OMI-derived summertime (April to September) NO_x emissions, the OMI-observed summertime NO₂ burdens at low (<3 m s⁻¹) speed winds condition, and the average summertime NO₂ concentrations at 13:00–14:00 LT in Chicago during 2006*–2013*. Error bars express the ±1 SD of the annually estimated results. *R* values shown are the correlation coefficients with the OMI-observed NO₂ burdens.

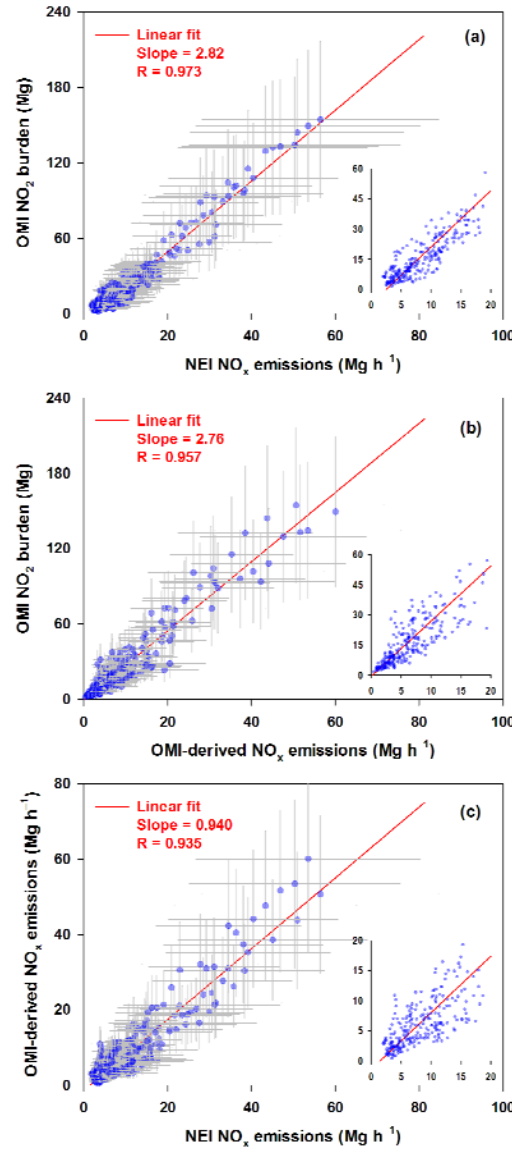


Fig. 6. Scatter plots of (a) OMI-observed NO₂ burdens at low ($<3 \text{ m s}^{-1}$) speed winds condition against NEI NO_x emissions, (b) OMI-observed NO₂ burdens against OMI-derived NO_x emissions, and (c) OMI-derived NO_x emissions against NEI NO_x emissions for 35 selected U.S. urban areas during 2005–2014. Each point represents a three-year result for an urban area. Error bars express the ± 1 SD uncertainties. Uncertainties of NEI emissions are set to be 50% according to the expert judgment. The inset figures are the zoomed views of points with emissions $<20 \text{ Mg h}^{-1}$.

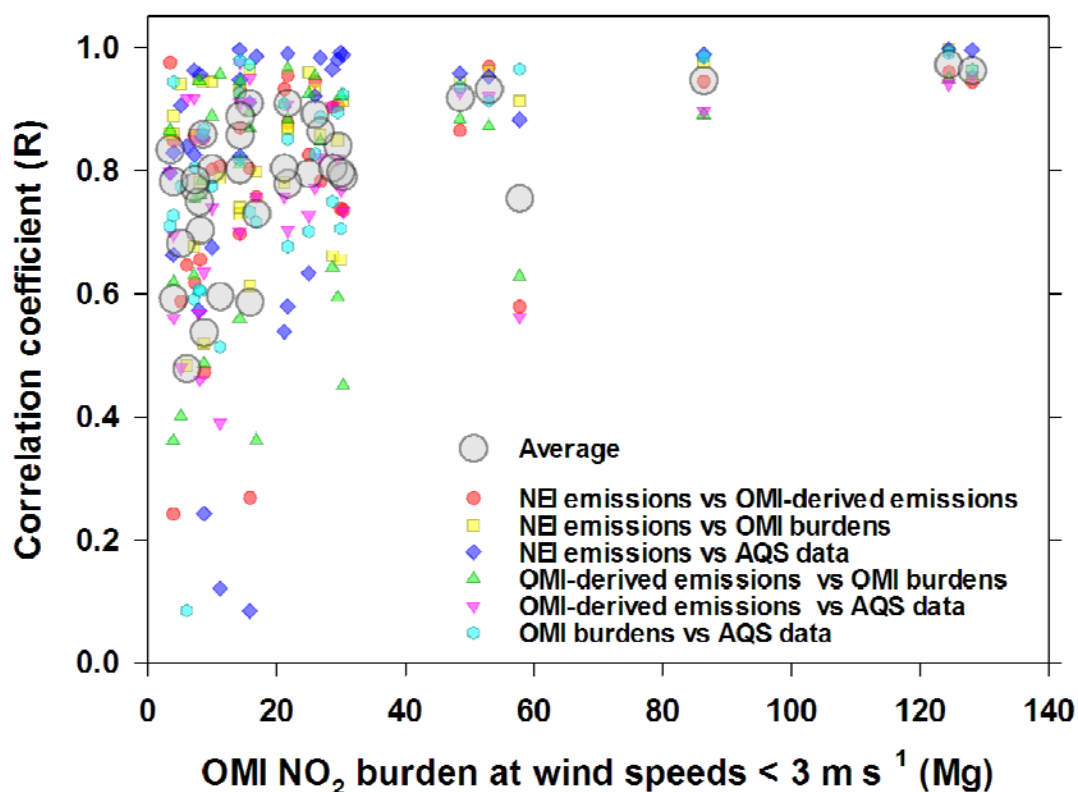


Fig. 7. Correlation coefficients of pair-wise trends among the NEI NO_x emissions, the OMI-derived NO_x emissions, the OMI NO₂ burdens at wind speeds <3 m s⁻¹, and the AQS NO₂ measurements against the mean OMI NO₂ burdens under the weak-wind speed condition (<3 m s⁻¹) for all selected urban areas during 2006*–2013*. Each large gray circle represents the average of the six correlation coefficients for an urban area.

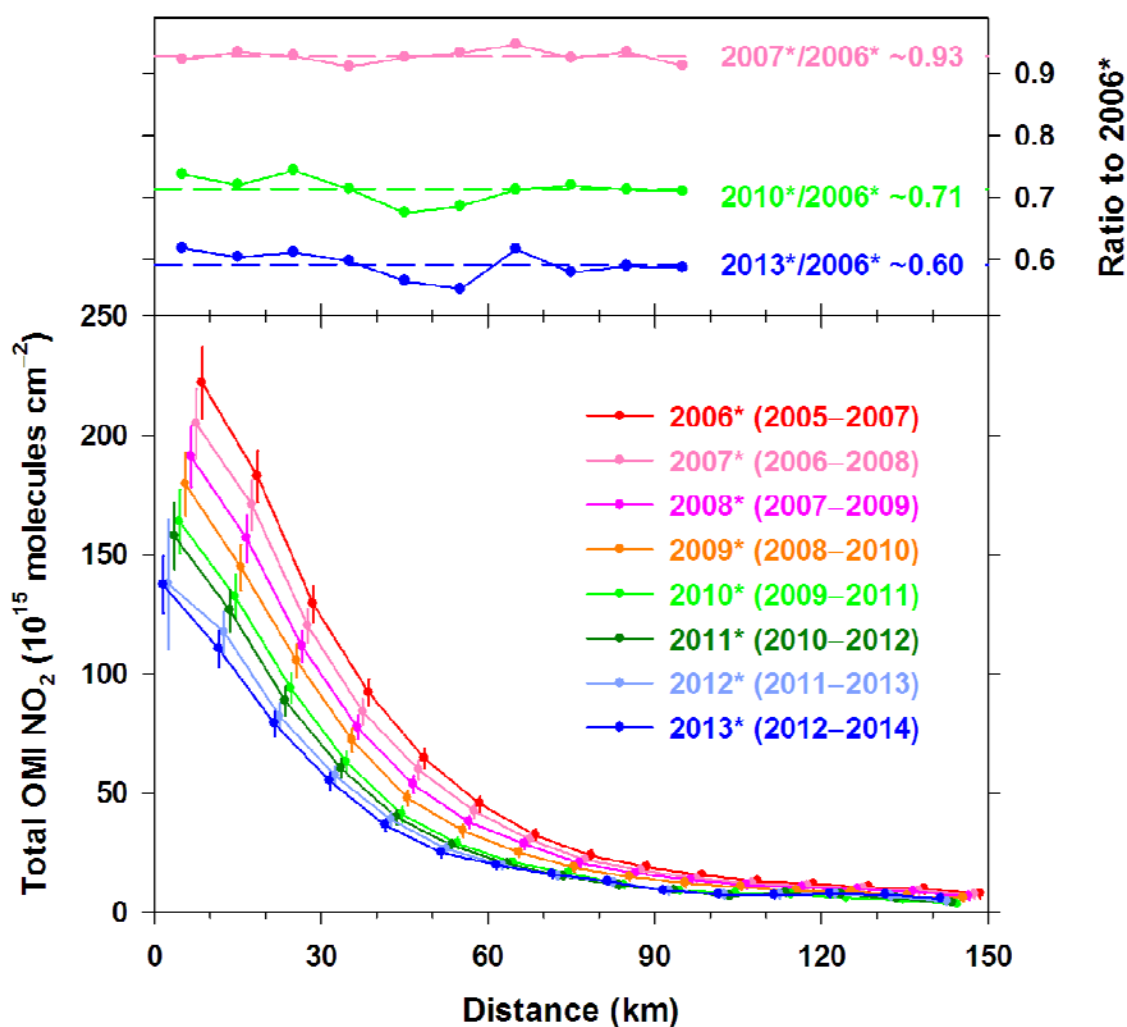


Fig. 8. The sum of three-year averaged OMI NO₂ TVCDs under the weak-wind speed condition for 35 selected U.S. urban areas as a function of the distance from the urban centers during 2006* to 2013*. The background NO₂ of urban areas was removed. Error bars express the 95% confidence intervals of the mean. The ratios of 2007* to 2006*, 2010* to 2006*, and 2013* to 2006* are shown at the top.

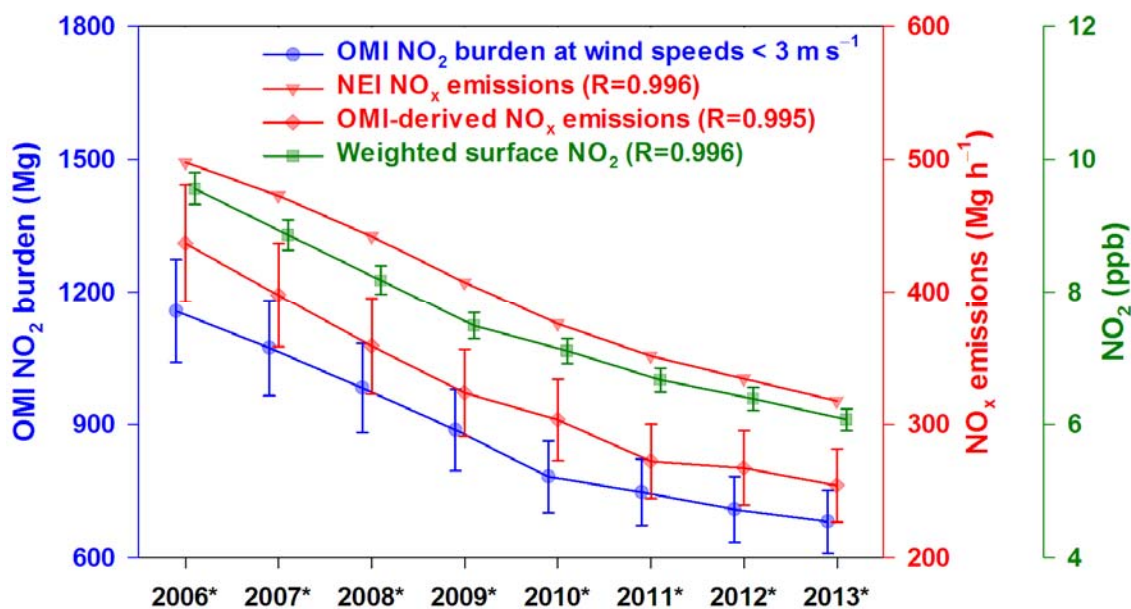


Fig. 9. Three-year moving trends of the total NEI NO_x emissions, the total OMI-derived NO_x emissions, the total OMI-observed NO₂ burdens under the weak-wind speed condition, and the area-weighted average AQS surface NO₂ measurements for all selected urban areas during 2006*–2013*. Error bars express the ± 1 SD of the estimates. *R* values shown are the correlation coefficients with the OMI-observed NO₂ burdens.

Table 1. Summary of the average bottom-up NO_x emissions, OMI-derived NO_x results, ground-based NO₂ measurements, and their linear trends for 35 U.S. urban areas during the summer half-year (April to September) from 2006* to 2013*. ^a

Urban Areas	Latitude	Longitude	NEI emissions 2005–2014 (Mg h ⁻¹)	Results at high wind speeds (WS)			Results at low WS		Linear trends from 2006* to 2013* (% yr ⁻¹)				Mean R ^b
				Mean WS (m s ⁻¹)	OMI-derived emissions (Mg h ⁻¹)	Effective lifetime (h)	Mean WS (m s ⁻¹)	OMI burden (Mg)	NEI emissions	OMI-derived emissions	OMI burden at WS <3 m s ⁻¹	AQS	
Atlanta, GA	33.74	-84.32	12.7	5.7	6.7±2.8	4.3±1.4	1.9	25.0±10.1	-7.9	-7.8±3.3	-15.3±6.2	-5.0	0.80
Boston, MA	42.38	-71.02	10.3	6.1	10.9±4.5	5.3±1.7	1.9	29.5±11.9	-6.1	-13.4±5.6	-8.1±3.3	-4.7	0.84
Charlotte, NC	35.34	-80.86	3.3	5.8	2.7±1.1	4.0±1.3	1.8	8.7±3.5	-1.3	-7.9±3.4	-12.9±5.2	-6.1	0.54
Chicago, IL	41.78	-87.68	30.7	7.4	23.3±9.7	6.1±1.9	2.1	86.3±34.8	-6.6	-7.8±3.3	-5.7±2.3	-6.8	0.95
Cincinnati, OH	39.12	-84.50	7.9	4.9	4.9±2.0	5.6±1.8	1.8	16.9±6.8	-3.9	-8.5±3.6	-6.0±2.5	-6.0	0.73
Dallas, TX	32.86	-96.96	14.8	7.4	8.1±3.4	3.3±1.1	2.0	26.8±10.8	-7.4	-12.2±5.1	-5.3±2.1	-7.3	0.86
Denver, CO	39.78	-105.04	10.0	6.0	12.1±5.0	3.5±1.1	1.8	21.7±8.8	-2.4	-9.8±4.1	-9.4±3.8	-2.1	0.78
Detroit, MI	42.26	-83.12	26.1	6.4	18.7±7.8	5.2±1.7	2.0	57.7±23.3	-6.6	-3.4±1.5	-5.8±2.3	-5.3	0.76
El Paso, TX	31.74	-106.38	2.2	6.7	3.2±1.3	3.0±0.9	1.9	7.2±2.9	-3.3	-3.7±1.6	-4.4±1.8	-4.6	0.77
Houston, TX	29.82	-95.28	13.5	5.9	11.3±4.7	4.1±1.3	1.9	30.3±12.2	-7.9	-5.2±2.3	-5.1±2.1	-4.8	0.79
Indianapolis, IN	39.80	-86.12	4.3	5.6	3.1±1.3	4.2±1.3	2.0	8.5±3.4	-3.2	-5.7±2.5	-6.5±2.6	-7.8	0.86
Jacksonville, FL	30.40	-81.60	5.2	5.7	4.7±2.0	2.5±0.8	1.9	9.9±4.0	-9.5	-6.3±2.8	-9.5±3.8	-2.9	0.80
Kansas City, MO	39.10	-94.56	10.2	6.6	5.1±2.1	3.9±1.2	1.9	14.3±5.8	-4.4	-7.8±3.3	-13.4±5.4	-4.9	0.86
Las Vegas, NV	36.18	-115.14	6.1	6.4	6.7±2.8	2.0±0.7	1.9	11.2±4.5	-3.3	-10.3±4.4	-12.3±5.0	-3.0	0.60
Los Angeles, CA	34.06	-117.92	40.1	3.7	40.0±16.6	3.6±1.2	2.0	124.4±50.2	-10.7	-7.0±2.9	-8.5±3.4	-7.6	0.97
Louisville, KY	38.20	-85.74	6.3	5.6	2.5±1.0	3.5±1.1	1.9	8.1±3.3	-7.6	-9.0±3.8	-11.3±4.6	-13.1	0.70
Memphis, TN	35.10	-90.04	4.4	5.9	1.5±0.6	3.2±1.0	1.9	3.4±1.4	-7.3	-25.9±10.8	-10.2±4.1	-2.7	0.83
Miami, FL	26.02	-80.34	13.4	5.4	5.6±2.3	5.0±1.6	1.9	28.7±11.6	-6.5	-10.2±4.3	-4.5±1.8	-9.3	0.80
Minneapolis, MN	44.96	-93.22	12.8	6.9	9.3±3.9	2.7±0.9	2.0	25.9±10.5	-8.6	-12.4±5.2	-11.3±4.6	-11.0	0.89
Nashville, TN	36.14	-86.62	2.9	5.6	2.0±0.8	2.8±0.9	1.8	4.0±1.6	-4.4	-13.8±5.8	-14.9±6.0	-6.9	0.78
New Orleans, LA	29.98	-90.22	7.2	5.3	3.6±1.5	3.2±1.0	1.8	6.0±2.5	-5.2	-7.3±3.2	-1.8±1.1	-5.4	0.48
New York, NY	40.72	-73.80	43.2	5.3	50.7±21.1	3.1±1.0	1.9	128.1±51.7	-6.3	-5.9±2.5	-6.8±2.8	-6.7	0.96
Philadelphia, PA	39.98	-75.16	17.8	5.2	23.3±9.8	3.2±1.0	1.9	53.0±21.4	-7.2	-9.1±4.0	-18.1±7.3	-7.2	0.93
Phoenix, AZ	33.54	-112.00	10.8	5.4	12.2±5.1	1.8±0.6	1.7	21.1±8.5	-4.7	-13.0±5.5	-6.4±2.6	-4.6	0.80
Portland, OR	45.44	-122.60	6.9	3.9	9.9±4.1	1.2±0.4	2.1	15.8±6.4	-3.8	-5.0±2.2	-11.6±4.7	-8.1	0.91
Richmond, VA	37.42	-77.30	3.6	4.9	1.8±0.7	3.5±1.1	2.0	5.1±2.1	-7.8	-5.7±2.7	-14.7±5.9	-9.4	0.68
Salt Lake City, UT	40.72	-111.92	3.6	4.8	8.2±3.5	1.3±0.4	1.8	14.3±5.8	-3.7	-12.1±5.4	-9.3±3.8	-10.8	0.89
San Antonio, TX	29.56	-98.44	5.4	5.7	3.2±1.4	2.1±0.7	2.0	7.9±3.2	-5.7	-10.2±4.4	-8.2±3.4	-1.6	0.75
San Diego, CA	32.66	-116.86	6.0	4.0	8.8±3.7	3.1±1.0	2.0	21.7±8.8	-9.8	-6.3±3.0	-4.2±1.7	-7.8	0.91
Seattle, WA	47.42	-122.22	13.0	3.7	13.3±5.7	3.4±1.1	2.0	30.0±12.1	-4.8	-6.5±3.3	-4.3±1.9	-5.6	0.80
St. Louis, MO	38.64	-90.32	11.0	5.2	4.9±2.0	6.8±2.1	1.9	15.8±6.4	-0.7	-10.9±4.5	-8.9±3.6	-10.0	0.59
Tampa, FL	27.90	-82.42	8.5	5.6	6.9±2.9	2.7±0.9	1.8	14.3±5.8	-9.5	-6.6±2.8	-9.1±3.7	-10.5	0.80
Tucson, AZ	32.24	-110.88	3.1	5.9	1.5±0.6	3.6±1.2	1.8	3.9±1.6	-6.0	-6.2±2.7	-4.0±1.7	-7.4	0.59
Virginia Beach, VA	36.90	-76.32	6.1	6.2	4.6±1.9	1.4±0.4	2.0	7.3±2.9	-8.7	-8.9±3.7	-8.7±3.5	-6.1	0.79
Washington, DC	39.20	-76.58	18.5	5.0	13.0±5.5	4.7±1.5	1.9	48.5±19.6	-7.3	-10.2±4.3	-6.9±2.8	-6.2	0.92

^a 2006* and 2013* denote the three-year average of 2005–2007 and 2012–2014, respectively.

^b Average correlation coefficients (*R*) of pair-wise trends among the NEI NO_x emissions, the OMI-derived NO_x emissions, the OMI NO₂ burdens, and the AQS NO₂ measurements.

1

2

3 Table 2. Summary of NO_x-related trends over all selected U.S. urban areas during 2006*–2013* ^a.

	2006*–2013*	2006*–2010*	2010*–2013*
Sum of OMI NO ₂ columns under winds <3 m s ⁻¹	-6.9% yr ⁻¹	-9.0% yr ⁻¹	-3.9% yr ⁻¹
Total NEI NO _x emissions	-6.2% yr ⁻¹	-6.8% yr ⁻¹	-4.9% yr ⁻¹
Total OMI-derived NO _x emissions	-7.4% yr ⁻¹	-8.7% yr ⁻¹	-3.4% yr ⁻¹
Total OMI NO ₂ burdens under winds <3 m s ⁻¹	-7.3% yr ⁻¹	-9.3% yr ⁻¹	-4.6% yr ⁻¹
Average NO ₂ concentrations	-6.3% yr ⁻¹	-7.2% yr ⁻¹	-4.6% yr ⁻¹

4 ^a 2006*, 2010*, and 2013* denote the three-year average of 2005–2007, 2009–2011, and 2012–2014, respectively.

5